Reevaluation of the cosmic antideuteron flux from cosmic-ray interactions and from exotic sources

Laura Šerkšnytė,[1,*] Stephan Königstorfer,[1,†] Philip von Doetinchem,[2] Laura Fabbietti,[1] Diego Mauricio Gomez-Coral,[2] Johannes Herms,[3] Alejandro Ibarra,[1] Thomas Pöschl,[1] Anirvan Shukla,[2] Andrew Strong,[4] and Ivan Vorobyev[1]

[1]*Department of Physics, Technical University of Munich, James-Franck-Straße, 85748 Garching, Germany*
[2]*Department of Physics and Astronomy, University of Hawaii at Manoa, 2505 Correa Road, Honolulu, Hawaii 96822, USA*
[3]*Max-Planck-Institut für Kernphysik, Saupfercheckweg 1, 69117 Heidelberg, Germany*
[4]*Max-Planck-Institut für extraterrestrische Physik, Giessenbachstraße, 85748 Garching, Germany*

(Received 8 January 2022; accepted 4 April 2022; published 27 April 2022)

Cosmic-ray antideuterons could be a key for the discovery of exotic phenomena in our Galaxy, such as dark-matter annihilations or primordial black hole evaporation. Unfortunately the theoretical predictions of the antideuteron flux at Earth are plagued with uncertainties from the mechanism of antideuteron production and propagation in the Galaxy. We present the most up-to-date calculation of the antideuteron fluxes from cosmic-ray collisions with the interstellar medium and from exotic processes. We include for the first time the antideuteron inelastic interaction cross section recently measured by the ALICE collaboration to account for the loss of antideuterons during propagation. In order to bracket the uncertainty in the expected fluxes, we consider several state-of-the-art models of antideuteron production and of cosmic-ray propagation.

DOI: 10.1103/PhysRevD.105.083021

I. INTRODUCTION

In recent years there has been a growing interest in searches for cosmic-ray antiparticles with space-based and balloon-borne experiments, like BESS, PAMELA, and AMS-02 [1–7]. One of the motivations is that rare antiparticles act as messengers for exotic processes in the Galaxy, such as dark-matter annihilation or decay [8–22], which have a very low astrophysical background at kinetic energies below few GeV/nucleon. This background is generated by interactions of primary cosmic rays, like protons or α particles, with the interstellar medium (ISM). The only cosmic-ray antiparticles that have been detected to date are positrons [23–25] and antiprotons [1–4,7]. The exquisite measurements of the positron and antiproton spectra are currently being actively interpreted and analyzed. The positron energy spectrum shows a hardening at high energies that cannot be explained by standard cosmic-ray propagation models, like GALPROP [26]. Explanations span a wide range of very different models from various acceleration mechanisms to positron production in pulsars and dark-matter annihilation [27]. For antiprotons, deviations from the standard cosmic-ray propagation prediction have also been found with varying degrees of significance [28–34]. Some of these antiproton studies suggest a dark-matter interpretation that can also explain the γ-ray excess observed in the Galactic Center [29,32]. However the deviations of the observed antiproton fluxes from the nonexotic background predictions are not very large. This poses a challenge for the interpretations, influenced by other uncertainties related to, e.g., antiparticle production cross sections for primary cosmic-ray interactions with the ISM, propagation parameters, solar modulation, or instrumental resolution effects.

In the search for cosmic messengers with a higher signal from exotic processes with respect to the astrophysical background, cosmic-ray antideuterons were proposed as a possible signature about 20 years ago [8], for recent reviews see [35,36]. Antideuterons are composed of one antiproton and one antineutron. From studies of light antinuclei production at particle colliders on Earth, it is known that the addition of one antinucleon to the antinucleus suppresses the production cross section by about a factor of 1000 in proton-proton collisions [37], resulting in the prediction of a much lower cosmic antideuteron flux with respect to antiprotons. Thus, in a fairly generic way, it is possible in a broad range of models, like dark-matter annihilation, to produce a cosmic antideuteron flux that is both several orders of magnitude above the astrophysical

*laura.serksnyte@tum.de
†s.koenigstorfer@tum.de

antideuteron background prediction and shows a different spectral shape with respect to the expected antideuteron background due to the underlying kinematics, but is also several orders of magnitude lower with respect to antiprotons. The detection of only one or a few cosmic antideuterons would be a potential breakthrough for finding imprints of exotic processes because they can be easily separated from other background antideuterons. The search requires experiments with large acceptance, long measurement time, and high particle identification power. The best exclusion limits have been reported by the BESS experiment collaboration [1], and the analysis of the currently operational multipurpose AMS-02 experiment aboard the International Space Station is ongoing. The upcoming balloon-borne experiment GAPS is a dedicated low-energy cosmic antinuclei search and is expected to have its first flight by the end of 2022 [38–40]. Interestingly, the AMS-02 collaboration reported several antihelium candidate events [41], which already generated broad theoretical interest, with no preferred explanation. However, the consensus seems to be that, if confirmed, then it would have a transformative impact on understanding the processes in the Galaxy. A confirmed detection of antihelium would also directly impact the predictions of the antideuteron flux. Therefore, any model explaining the potential cosmic antihelium signal must not be above the measured antiproton flux and must respect current antideuteron detection limits.

The properties of light cosmic-ray antinuclei have been studied in accelerator-based experiments using various colliding systems and colliding energies to determine their production mechanisms quantitatively [42–60]. Despite the plethora of very precise measurements, the studies do not suffice to constrain the antinuclei production cross sections within the very wide energy range of collisions occurring between high-energy cosmic rays and nuclei present in the interstellar medium. Hence relatively large uncertainties of about a factor of 10 are still present in the most critical energy region [61]. Thus more measurements of this kind are needed, and especially more comprehensive modeling of the antinuclei production in hadron-hadron collisions is necessary [62,63]. Accelerator-based experiments not only constrain the yield of secondary antinuclei in our Galaxy but also set essential boundaries on the dark-matter annihilation processes resulting in the production of antinuclei (e.g., [12,64]). Another crucial aspect that can be studied at accelerators is the inelastic interaction cross section of light antinuclei with matter. Such processes play a fundamental role in the propagation of antinuclei for cosmic-ray experiments. Recently measurements of the inelastic cross section of antideuterons [65] have been performed over a wide momentum range, and they can now be used as input to propagation programs. Several additional experimental efforts are underway to reduce the related uncertainties using new data from the ALICE [65] and NA61/SHINE [66] experiments.

After introducing potential antinuclei sources (Sec. III), this study focuses on using the latest data and models for antinuclei production and interaction cross sections together with up-to-date cosmic-ray propagation models (Secs. II and IV) for a prediction of exotic signal and background antideuteron fluxes.

II. COSMIC-RAY PROPAGATION

Relativistic nuclei, and electrons and positrons, pervade our Galaxy and are collectively known as cosmic rays. They span energies from MeV to PeV and above. Detailed expositions of cosmic-ray transport is given in [67,68]; here we summarize the essential concepts. Galactic cosmic rays are thought to originate mainly from diffusive shock acceleration of interstellar gas by supernova remnants, with other sources like pulsars and pulsar wind nebulae possibly also contributing.

Cosmic rays from such sources are referred to as primary; they interact with the hydrogen (H) and helium (He) atoms within the interstellar medium to produce secondary nuclei and antinuclei. For example, a spallation process converts a primary carbon nucleus (C, $Z = 6$, $A = 12$, 13) into a secondary boron nucleus (B, $Z = 5$, $A = 10$, 11). Cosmic-ray nuclei cover the full range of isotopes from H through He to Ni, and secondary antinuclei and antideuterons.

Cosmic rays propagate in the Galaxy mainly through diffusion due to scattering on interstellar turbulence and convection by Galactic winds. They eventually leave the Galaxy, filling a region known as the cosmic-ray halo which has a vertical extent of several kpc. Their residence time in the Galaxy is about 10–100 Myr. Their energy is lost by hadronic interactions such as pion production and ionization. Inelastic collisions and radioactive decay are further loss mechanisms. The cosmic-ray propagation is described by the Fokker-Planck equation, which can be written as

$$\frac{\partial \psi}{\partial t} = Q(\boldsymbol{r}, p) + \mathbf{div}(D_{\mathrm{xx}}\mathbf{grad}\psi - \boldsymbol{V}\psi) + \frac{\partial}{\partial p} p^2 D_{\mathrm{pp}} \frac{\partial}{\partial p} \frac{\psi}{p^2} - \frac{\partial}{\partial p}\left[\psi \frac{\mathrm{d}p}{\mathrm{d}t} - \frac{p}{3}(\mathbf{div} \cdot \boldsymbol{V})\psi\right] - \frac{\psi}{\tau}, \quad (1)$$

where $\psi = \psi(\boldsymbol{r}, p, t)$ is the time-dependent cosmic-ray density per unit of the total particle momentum at position $\boldsymbol{r}$. $Q(\boldsymbol{r}, p)$ is the source term of the cosmic rays, which can include primary particles injected by supernova remnants, secondaries coming from spallation and cosmic-ray collisions with the interstellar medium as well as more exotic sources such as dark-matter annihilation. D_{xx}, $\mathbf{V}$, and D_{pp} are the spatial diffusion coefficient, the convection velocity, and the diffusive reacceleration coefficient, respectively, and are called propagation parameters.

The last term ψ/τ accounts for particles lost via decay, fragmentation and inelastic interactions in the Galaxy.

Solar modulation is significant below about 1 GeV/nucleon kinetic energy per nucleon and is treated separately using the force field approximation [69] or with special codes such as HelMod [70,71].

In this work the GALPROP program [6,72,73] is used to compute cosmic-ray propagation. In this setup, our Galaxy is approximated as a cylinder with a halo height of 4 kpc and a radius of 20 kpc. The distribution of cosmic-ray sources in the Galaxy is based on supernova remnants, but pulsars are used since the supernova distribution is very uncertain. Pulsars should have a similar distribution to supernova remnants, but more observations of pulsars are available, and their distances are measured more precisely. The source distribution is thus parametrized as a function of galactocentric radius based on pulsars and an exponential behavior above and below the Galactic plane with a scale length of order 100 pc. The cosmic-ray injection spectrum can be parametrized as a power-law in momentum, $p^{-\alpha}$, where the spectral index α is momentum dependent and assumes typical values of $\alpha = 2.3$ above a few GeV, flattening to 1.8 at lower momenta. Isotopic abundances of primary cosmic rays are fixed in GALPROP by the cosmic-ray flux values measured at 100 GeV/nucleon kinetic energy because solar modulation does not affect this energy range. The halo height z_h, at which cosmic rays are assumed to fall to zero, is a free parameter with values between 1 and 20 kpc, and it is determined from the fit to cosmic-ray data carried out to fix the propagation parameters. The propagation parameters are determined by exploiting the relation between primary and secondary cosmic rays observed by experiments on balloons and satellites. Since the primary cosmic-ray spectrum can be measured and the cross sections for the secondary production are known, the primary-to-secondary ratios can be used to constrain the propagation parameters. The parameters are determined by fitting the primary H and He spectra, the boron-to-carbon ratio (B/C), and other secondary-to-primary ratios [6].

Convection by the Galactic wind is specified by the convection velocity, which is assumed to have a linear increase with distance from the plane. It must be equal to 0 at the Galactic plane to avoid a discontinuity there. The diffusion coefficient can be parametrized as $D_{xx} = \beta R^{-\alpha}$, where $\beta = v/c$, v is velocity, c is the speed of light, and $R = pc/eZ$ is the rigidity. The β term reflects that diffusion depends on the speed with which particles scatter on interstellar turbulence. Astronomical information such as the distribution of atomic and molecular gas in the Galaxy for spallation, the interstellar radiation fields for leptonic interactions are based on large-scale surveys at various levels of detail.

The present work is based on GALPROPv56 [72] with various modifications because the propagation of antinuclei (apart from antiprotons) was not included in GALPROP before this work. Full technical details of the GALPROP parameters and solution methods, with diagnostics of the solution, together with illustrative analytical solutions, can be found in the GALPROP explanatory supplement.[1]

TABLE I. The main propagation parameters used in GALPROP. For full parameter sets refer to Boschini *et al.* and Cuoco *et al.*

Parameter	Units	Boschini *et al.*	Cuoco *et al.*
z_h	kpc	4	6.78
D_0	$\mathrm{cm^2\,s^{-1}}$	4.3×10^{28}	7.48×10^{28}
δ^a		0.415	0.361
V_{alf}	$\mathrm{km\,s^{-1}}$	30	23.8
V_{conv} $(z = 0$ kpc)	$\mathrm{km\,s^{-1}}$	0	26.9
$\mathrm{d}V_{conv}/\mathrm{d}z$	$\mathrm{km\,s^{-1}\,kpc^{-1}}$	9.8	0

Despite the complex framework of GALPROP, it is important to note that secondary production of antiprotons and antideuterons is determined mainly by the (momentum-dependent) "grammage" or column of matter traversed, not directly by the halo size, since the latter only affects radioactive species via the residence time. The well-measured B/C ratio as a function of energy determines the grammage. Any combination of D_{xx} and halo size, which gives the correct B/C that can be used, at least to a good approximation; B/C constrains only[2] z_h/D_{xx}.

In this work, the relevant antideuteron source functions and the characteristic inelastic cross sections have been implemented in GALPROP to estimate the antideuteron fluxes. The details can be found in Secs. III and IV. The propagation parameters obtained in Boschini *et al.* (P scenario) [72] (Table I) have been used, and the kinetic-energy grid employed in GALPROP has been adapted to the available antideuteron production cross sections. To illustrate the uncertainty of GALPROP propagation parameters, the Cuoco *et al.* parametrization is employed as well (Table I).

III. ANTINUCLEI PRODUCTION IN THE GALAXY

The first step of our study consists in the evaluation of the different antideuteron sources in the Galaxy. We consider here three main components: one stemming from the collisions of cosmic rays with the interstellar medium, one due to weakly interacting massive particle (WIMP) dark-matter annihilations, and one from primordial black hole evaporation. The production of antideuterons is studied and interpreted at accelerator-based experiments by means of statistical hadronization or coalescence models. In the first approach, particles are produced from a fireball at thermal equilibrium with temperatures close to 156 MeV for collisions at the LHC and their abundance is fixed at the

[1]https://gitlab.mpcdf.mpg.de/aws/galprop.

[2]https://gitlab.mpcdf.mpg.de/aws/galprop: Explanatory Supplement, Eq. (63).

chemical freeze-out, when the inelastic collisions cease [74]. In this scenario it is improbable that "fragile" objects as deuterons (binding energy = 2.2 MeV) can survive the hot system created at RHIC or LHC, but the measured (anti) nuclei yields are reproduced by the existing models [75]. It is clear however, that such models do not provide any detailed information on momentum distribution of the formed antideuterons and are also not suited to extract a general formalism for the production of (anti)nuclei in hadron–hadron collisions at energies between 17 GeV (antideuteron production threshold in p-p collisions) and several TeV. This very broad energy range characterizes the production of antideuterons in our Galaxy by collisions of cosmic rays with the nuclei in the interstellar medium. Coalescence models, on the other hand, provide predictions for both the yields and momentum spectra of the produced light antinuclei and can be applied to the full energy range. Thus, in this work we consider only coalescence models.

A. Antinuclei formation with coalescence models

There is no first-principle calculation of antideuteron production cross sections in low-energy proton-proton collisions or hypothetical dark-matter annihilation processes. Therefore, any prediction of antideuteron fluxes needs to rely on experimental data. As antideuteron production is a rare process, experimental data are scarce, and a purely data driven approach is unfeasible. Instead one has to rely on physically motivated models of antinuclei coalescence to extrapolate the available data. The degree of confidence in the final result then depends both on the experimental data, as well as on the plausibility of the model.

The separation of energy scales justifies treating antideuteron production as the coalescence of two antinucleons produced in some high-energy process. Under the assumption that antineutrons and antiprotons are produced uncorrelated, the antideuteron yield of a process can be estimated by factorized coalescence [11,76] as

$$E_{\bar{\mathrm{d}}}\frac{\mathrm{d}^3N_{\bar{\mathrm{d}}}}{\mathrm{d}p_{\bar{\mathrm{d}}}^3} \simeq B_2\left(E_{\bar{\mathrm{p}}}\frac{\mathrm{d}^3N_{\bar{\mathrm{p}}}}{\mathrm{d}p_{\bar{\mathrm{p}}}^3}\right)\left(E_{\bar{\mathrm{n}}}\frac{\mathrm{d}^3N_{\bar{\mathrm{n}}}}{\mathrm{d}p_{\bar{\mathrm{n}}}^3}\right) \tag{2}$$

$$\simeq B_2\left(E_{\bar{\mathrm{p}}}\frac{\mathrm{d}^3N_{\bar{\mathrm{p}}}}{\mathrm{d}p_{\bar{\mathrm{p}}}^3}\right)^2, \tag{3}$$

where p_i and $\mathrm{d}N_i/\mathrm{d}p_i$ are the momentum and the differential yield of particle i. Here, B_2 is the coalescence parameter, which can be related to a momentum-space coalescence condition: a pair of anti-nucleons produced in the same high-energy process coalesces into an antideuteron if the anti-nucleons' relative momentum in the pair's center-of-mass frame is less than the coalescence momentum, $|\vec{p}_{\bar{\mathrm{p}}} - \vec{p}_{\bar{\mathrm{n}}}| < p_0$. In the analytical factorized coalescence model, this is equivalent to [77,78]

$$B_2 = \frac{1}{8}\frac{4\pi p_0^3}{3}\frac{m_{\bar{\mathrm{d}}}}{m_{\bar{\mathrm{p}}}^2}. \tag{4}$$

Since the B_2 parameter can be measured [79], it is possible to determine the p_0 parameter, which will vary as a function of the colliding system and colliding energy.

Going beyond the factorized coalescence model, an event-by-event procedure based on the Monte Carlo production of antinucleons in particle collisions followed by the coalescence of antiproton-antineutron pairs takes into account correlations between the antinucleons [12–14,77]. Here, in addition to the momentum-space coalescence criterion, the coalescing antinucleons are required to be close in position space, excluding antinucleons produced in weak decays from coalescing with those produced promptly. The coalescence momentum is then determined by comparison to experimental data, where it is found that different values are needed to accommodate results in different particle physics processes [35] or even at different process energies [61]. The degree of confidence in the final antideuteron yield then depends both on the event generator's ability to accurately simulate antinucleon production and correlation, as well as on the coalescence condition. The simplifying assumption of uncorrelated production of antiproton and antineutron in the factorized coalescence model has clear limits, and different experimental results require vastly different values of B_2 and p_0 [61,77].

A more advanced parametrization of the dependence between B_2 and p_0 has been investigated by including the size of the formed antinuclei relative to the size of the particle-emitting source formed after the hadron collisions [80]. The size effect is found to be more important for large colliding systems such as Pb-Pb. However, since the size of the particle emitting source depends on the antinuclei transverse momentum [81], the interplay between the nuclei size and source size should ideally be considered also in p-p collisions. More sophisticated approaches in this direction [62,82] study the connection between final-state interactions and resulting two-particle correlations for antinucleons and coalescence models. The derived correlation-coalescence relation takes into account both the antinuclei wave functions and colliding system's properties and the size of the particle emitting source. Recently, a Wigner-function based, semiclassical model has been developed [83]. Given an ansatz for the antideuteron wave function, the antideuteron yield depends on the spatial spread σ of the produced antinucleons, which is fit to antideuteron data. In this model, a single value $\sigma \simeq 1$ fm explains antideuteron data from different processes and energies [63].

In this work, we use the antideuteron production cross sections in p-p collisions determined in [61,84], hereafter called Shukla *et al.*, and [63], hereafter called Kachelrieß *et al.* In Shukla *et al.* the formation of (anti)deuterons has

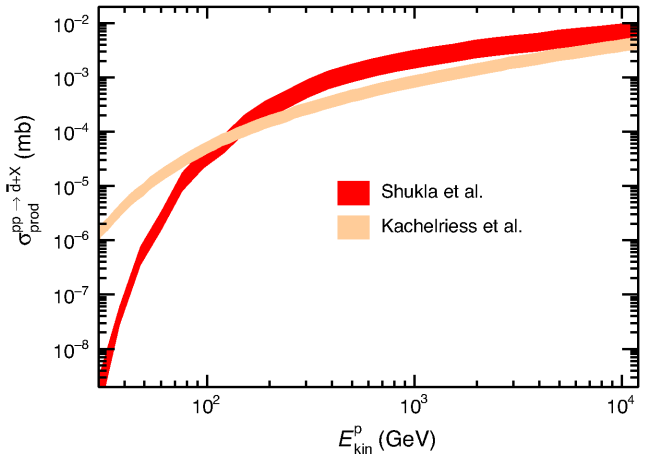

FIG. 1. Antideuteron total production cross section, in p-p collisions, as a function of the projectile kinetic energy $E^{\mathrm{p}}_{\mathrm{kin}}$ (GeV) in the laboratory frame for two models [61,83,84]. The band width corresponds to the uncertainty of the coalescence parameter. See text for details.

been studied using multiple Monte Carlo event generators, settling on EPOS-LHC [85] for its consistency with antiproton-production data in a wide range of energies. The p_0 parametrization for antideuteron production using EPOS-LHC has been found to depend on the collision energy, initially growing rapidly after the antideuteron production threshold, and finally reaching a saturation value of $p_0/2 = 89.6$ MeV at high energies. Figure 1 shows the total production cross section for antideuterons as a function of collision kinetic energy predicted by these two models. In both cases the bands represent the uncertainty derived from the limited knowledge of the coalescence parameters values (p_0 or σ) after being fitted to data. These uncertainties range from 10% for Kachelrieß *et al.* to 30% for Shukla *et al.* The two approaches use different event generators and consider slightly different datasets, which results in different final cross sections. At low energy (< 100 GeV/nucleon), data from Serpukhov [86] was included only in the study by Shukla *et al.* This dataset showed a lower antideuteron yield than was expected from observations at higher energies [61]. At high energies (> 200 GeV/nucleon), p_0 in Shukla *et al.* is obtained by including data on antideuteron and antihelium production up to $\sqrt{s} = 7$ and 13 TeV [61,84]. The comparatively smaller results obtained by Kachelriess *et al.* around 1000 GeV may be related to the underproduction of antinucleons in QGSJET-II at those energies, with associated uncertainties not quantified by [63]. More measurements of antiproton and antideuteron production cross sections in p-p and p-He collisions are necessary to tune event generators and improve antinuclei formation models.

For the antideuteron production in dark-matter annihilation and primordial black hole evaporation, we employ results from [12,87], to which we refer for a detailed discussion. These were determined using the event generator PYTHIA8.176 [88]. There are no data on antideuteron spectra from hypothetical dark-matter annihilation to fix the coalescence momentum p_0, which is instead determined from data on Standard Model processes expected to hadronize similarly (i.e., nonhadronic initial states producing electroweak gauge bosons or quark-antiquark pairs). In this spirit, the central value determined from ALEPH data on the antideuteron yield of Z decays [52] has been used, $p_0 = 192$ MeV, with an uncertainty bracketed by the 2σ allowed values determined from ALEPH and *BABAR* data [89] (the latter on antideuteron production from e^+e^- collisions at $\sqrt{s} = 10.58$ GeV): $p_0 = 128.7$–226.1 MeV [12].

B. Cosmic-ray collisions with interstellar medium

As described above, cosmic-ray antinuclei are expected to be produced by the interaction of primary cosmic rays, mostly protons and helium nuclei, with the ISM, also composed primarily of hydrogen and helium. Cosmic-ray antideuterons can be formed when the center-of-mass energy of the nucleon-nucleon collision induced by cosmic rays is above an energy threshold of $\sqrt{s} \approx 6$ GeV. Such antideuterons constitute the secondary source term. Although the antideuteron production cross section increases with the collision energy, the steeply declining cosmic-ray proton spectrum causes the antideuteron production to decrease at high energies. The contributions to the antideuteron source term from cosmic-ray protons of different kinetic energies is shown in the upper panel of Fig. 2 for p-H collisions. One can see that the largest contribution to the antideuteron yield comes from cosmic-ray energies around 300 GeV. The secondary source term $Q^{\mathrm{sec}}_{\bar{\mathrm{d}}}$ to be included in the transport Eq. (1) is calculated using

$$Q^{\mathrm{sec}}_{\bar{\mathrm{d}}}(\boldsymbol{r}, E^{\bar{\mathrm{d}}}_{\mathrm{kin}}) = \sum_{i=\mathrm{p,He},\bar{\mathrm{p}}} \sum_{j=\mathrm{p,He}} 4\pi n_j(\boldsymbol{r}) \times \int_{E^i_{\mathrm{kin,min}}}^{\infty} \mathrm{d}E^i_{\mathrm{kin}} \left(\frac{\mathrm{d}\sigma_{\mathrm{prod}}}{\mathrm{d}E^{\bar{\mathrm{d}}}_{\mathrm{kin}}}\right)_{ij} \Phi_i(\boldsymbol{r}, E^i_{\mathrm{kin}}). \quad (5)$$

Here the index i represents all the incident cosmic-ray species with flux Φ_i and kinetic energy per nucleon E^i_{kin}. Index j represents the ISM components with number densities $n_{\mathrm{p}} = 0.9$ cm^{-3} and $n_{\mathrm{He}} = 0.1$ cm^{-3} used to calculate source functions shown on the lower panel of Fig. 2. When using the GALPROP code, the standard implementation of gas distributions in the Galaxy is used, which is based on the available HI and CO surveys as well as the information on ionized compontent [90]. The secondary source term convolves the antideuteron differential production cross section $(\mathrm{d}\sigma_{\mathrm{prod}}/\mathrm{d}E^{\bar{\mathrm{d}}}_{\mathrm{kin}})_{ij}$ with the primary cosmic-ray fluxes involved in the collision.

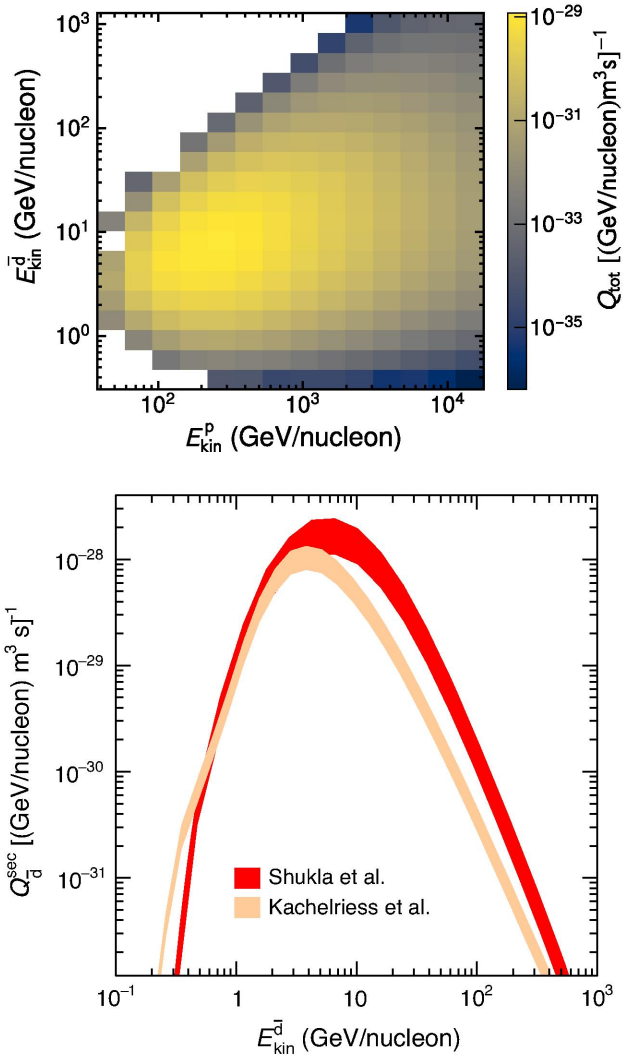

FIG. 2. Upper panel: contributions to the local source term $Q^{\rm sec}_{\bar{\rm d}}(E^{\bar{\rm d}}_{\rm kin})$ by incoming proton energy $E^{\rm p}_{\rm kin}$.The source term includes only p-H collisions. Lower panel: antideuteron source term, integrated over proton, helium and antiproton fluxes, as a function of its kinetic energy per nucleon for the two models described in Sec. III A. The source term on the lower panel includes antideuterons produced in p-H, p-He, He-p, $\bar{\rm p}$-p, and $\bar{\rm p}$-He collisions.

The source term is used in Eq. (1) to calculate the propagated secondary antideuteron flux using GALPROP.

In Ref. [84], $Q^{\rm sec}_{\bar{\rm d}}$ was estimated by simulating p-p interactions using EPOS-LHC as part of the CRMC [91] package at 27 logarithmically spaced collision energies between 31 GeV and 12.5 TeV in the laboratory frame. Since p-p collisions contribute 60%–70% of the total antinuclei source terms [16,92], only those have been simulated. The p-He, He-p, and He-He contributions have been estimated by scaling the parametrization developed in Ref. [30]. The differential production cross section has to be implemented in GALPROP in logarithmic kinetic energy per nucleon bins for protons and antideuterons. For this purpose the results from [84] have been interpolated using a cubic polynomial. An additional contribution to the antideuteron source term, especially important at low energies, is the interaction of cosmic-ray antiprotons with the ISM. This contribution was taken into account by simulating antideuteron production in $\bar{\rm p}$-p and $\bar{\rm p}$-He collisions using EPOS-LHC [92]. In Ref. [63], the antideuteron production in all collision systems (p-H, p-He, He-p, $\bar{\rm p}$-p, and $\bar{\rm p}$-He) was estimated using QGSJET-II. The lower panel of Fig. 2 shows the resulting secondary antideuteron source term, integrated over proton, helium and antiproton fluxes, as a function of the kinetic energy per nucleon for Shukla *et al.* [61,84] and Kachelrieß *et al.* [63]. The discrepancies observed between the two source terms below 0.5 GeV/nucleon and above 3 GeV/nucleon are a consequence of the disagreement in cross section described in the last section. The width of the two bands corresponds to the uncertainty in the coalescence model (see Sec. III A).

C. Dark matter

There is compelling evidence from multiple astronomical and cosmological observations for the presence of large amounts of dark matter in the Universe and our Galaxy (e.g., [93]). If dark matter consists of particles that can annihilate into Standard Model particles, as is generically expected for WIMPs produced through thermal freeze-out in the early Universe, it constitutes a potential source of cosmic-ray antideuterons. The source term for cosmic-ray antideuterons from dark-matter annihilations is

$$Q^{\rm DM,ann}_{\bar{\rm d}}(\boldsymbol{r}, E^{\bar{\rm d}}_{\rm kin}) = \frac{1}{2}\left(\frac{\rho(\boldsymbol{r})}{m_{\rm DM}}\right)^2 \langle\sigma v\rangle_f \frac{{\rm d}N^{\bar{\rm d}}_f}{{\rm d}E^{\bar{\rm d}}_{\rm kin}}, \qquad (6)$$

where $\rho(\vec{r})$ is the local dark-matter density in the Galaxy, $\langle\sigma v\rangle_f$ is the velocity averaged dark-matter annihilation cross section into channel f, for example $\rm b\bar{b}$ or W^+W^-, and ${\rm d}N^{\bar{\rm d}}_f/{\rm d}E^{\bar{\rm d}}_{\rm kin}$ is the antideuteron multiplicity produced from one such annihilation event. These are examined in turn in the following.

The Galactic dark-matter distribution $\rho(\vec{r})$ can be determined from kinematic tracers [94]. There is uncertainty both in the local density at the position of the Sun $r_\odot$, as well as in the shape of the distribution towards the inner Galaxy. To bracket the uncertainty due to the dark-matter profile, we consider the cuspy Navarro-Frenk-White [95] profile $\rho_{\rm NFW}(\vec{r}) \propto (r/r_s)^{-1}(1+r/r_s)^{-2}$ with scale radius $r_s = 24.4$ kpc. We also consider the flatter isothermal profile [96] $\rho_{\rm isothermal}(\vec{r}) \propto (r^2+r_s^2)^{-1}$ with scale radius $r_s = 4.38$ kpc, as well as the very cored Einasto profile [12] $\rho_{\rm Einasto} \propto \exp\left(-\frac{2}{\alpha}[(r/r_s)^\alpha - 1]\right)$ with scale radius $r_s = 28.44$ and $\alpha = 0.17$. These are normalized to a local dark-matter mass density of $\rho_\odot = 0.4$ GeV/cm^3, which is uncertain by up to a factor of 2 [97]. The profiles are shown in Fig. 3.

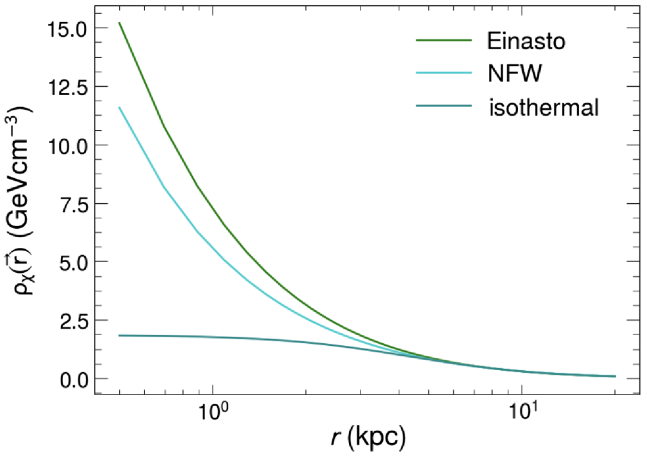

FIG. 3. The dark-matter density profiles, as a function of distance from the Galactic Center.

The value of the dark-matter annihilation cross section is not known. In the freeze-out scenario of particle dark-matter production, the dark-matter relic abundance today predicts a value $\langle\sigma v\rangle_{\rm thermal} \sim 2 \times 10^{-26}$ cm^3/s in the early Universe (e.g., [98]). In this context, the dark-matter mass $m_{\rm DM}$ is expected to be in the GeV–TeV range, with lower masses typically affected by constraints on dark-matter annihilation during recombination [99] and larger masses in conflict with unitarity [100]. To be relevant in the context of cosmic-ray antideuterons, the dark-matter mass needs to lie in the GeV range, with smaller masses unable to produce antideuterons, while the overall annihilation rate drops as $m_{\rm DM}^{-2}$.

Motivated by reports of tentative $^3\overline{\rm He}$ candidate events at relative high energies by the AMS-02 collaboration [101–103], other decays channels were recently considered. $\bar{\Lambda}_{\rm b}$ decays into antinuclei have received increasing attention, and it has been shown that they may increase the flux of antideuterons from dark matter by up to a factor of 4 [104] (see however [64,105]).

In the following, results for several benchmarks are shown intended to illustrate a range of antideuteron fluxes that can realistically be expected. The spectra are determined by dark-matter mass and annihilation channel, for which we choose $m_{\rm DM,b\bar{b}} = 10, 51, 100, 1000$ GeV and $m_{\rm DM,WW} = 94, 100, 1000$ GeV. The normalization is essentially determined by the annihilation cross section $\langle\sigma v\rangle$. There are strong constraints as well as contentious signal hints [30,32,34,106] on $\langle\sigma v\rangle$ from antiproton measurements by the AMS-02 detector [7]. These however depend significantly on the modeling of the antiproton production cross section, the propagation model, as well as experimental uncertainties that are yet to be fully characterized by the AMS-02 collaboration. We choose a conservative approach, adopting the theoretical expectation of $\langle\sigma v\rangle_{\rm thermal} \sim 2 \times 10^{-26}$ cm^3/s, which is not conclusively ruled out by antiproton measurements for dark-matter masses between ~50–100 GeV, while for the 10 GeV benchmark we adopt $\langle\sigma v\rangle = 3 \times 10^{-27}$ cm^3/s. These values are compatible with gamma ray limits from dwarf spheroidal galaxies [107]. Since $\langle\sigma v\rangle$ only affects the normalization, our results are easily translated to different values. We also propagate injection spectra determined by [104] with enhanced antideuteron production in $\bar{\Lambda}_{\rm b}$ decay: (i) 67 GeV dark matter annihilating into $\bar{\Lambda}_{\rm b}$ directly and (ii) 80 GeV dark matter annihilating into 14 GeV light mediators which then decay into $\bar{\Lambda}_{\rm b}$.

D. Primordial black holes

Primordial black holes (PBHs) could have been formed in the early Universe [108,109] and constitute a fraction of the cold dark matter abundance today. Their signatures today depend crucially on their mass. If they are sufficiently light, $M \lesssim 5 \times 10^{14}$ g, they are predicted to evaporate through Hawking radiation [110,111] on the timescale of the age of the Universe. The energy scale of the emitted particles is given by the Hawking temperature $T \approx 1.06\ {\rm GeV}/(M_{\rm PBH}/10^{13}\ {\rm g})$, evidently sufficient to produce antinuclei for such light PBHs.

Antideuteron source spectra from PBH evaporation have been computed in the event-by-event coalescence model as described in [87]. These are obtained by integrating the instantaneous Hawking emission rate of a single PBH over the PBH mass distribution today. While the initial mass function of PBHs produced in the early Universe is model dependent, the mass spectrum of PBHs capable of producing antideuterons today is determined solely by the mass loss rate. The predicted antinuclei spectra $Q(E^{\bar{\rm N}}_{\rm kin})$ are hence completely fixed by Hawking evaporation, and normalization is the only free parameter.

The normalization of the antideuteron source term $Q_{\rm PBH}(T, \vec{r})$ from PBH evaporation is linked to the PBH number density. PBHs constitute a form of cold dark matter, and one can assume their number density in the Galaxy follows that of DM, $Q_{\rm PBH}(E^{\bar{\rm d}}_{\rm kin}, \vec{r}) \propto Q_{\rm PBH}(E^{\bar{\rm d}}_{\rm kin}) \cdot \rho_{\rm DM}(\vec{r})$. Assuming a particular initial PBH mass function, ${\rm d}N/{\rm d}M \propto M^{-5/2}$ [112], the overall normalization is fixed by the local PBH mass density (or equivalently, the fraction of dark-matter in form of these PBHs). The results for $\rho_{\rm PBH} = 4 \times 10^{-11} \rho_{\rm DM}$ are shown here, which was found to be marginally compatible with antiproton limits in [87].[3]

[3]As the remaining lifetime of a BH with GeV temperature is only ~10^4 yr, the population of antinuclei-emitting PBHs can also be characterized by the local rate of explosive final PBH evaporation events. Our antinuclei spectra correspond to a local explosion rate of 3×10^{-4} pc^{-3} yr^{-1}.

IV. ANTIDEUTERON INELASTIC CROSS SECTION

After antideuterons are formed, their inelastic interactions with the ISM lead to a reduction of their flux, so the determination of the corresponding cross sections is a crucial aspect in flux calculations. The probability of an inelastic interaction is determined by the total nuclear inelastic cross section $\sigma_{\rm inel}^{\bar{\rm d}}$, which includes all processes leading to the disappearance of antideuterons (such as annihilation, nuclear breakup, charge exchange etc.).

The measurement of the inelastic cross section typically requires a beam of particles of interest (with well-determined momentum) and a target of known material composition and thickness. Since it is very challenging to obtain a beam of antideuterons with precise momentum, the knowledge of $\sigma_{\rm inel}^{\bar{\rm d}}$ was until recently very limited. For nearly 50 years the only available measurements of $\sigma_{\rm inel}^{\bar{\rm d}}$ came from the experimental facilities at the U-70 proton synchrotron. There, $\sigma_{\rm inel}^{\bar{\rm d}}$ was measured on various material targets (Li, C, Al, Cu, and Pb) for antideuterons with momenta of 13.3 GeV/c [113] and 25 GeV/c [114].

In high-energy collisions between protons and lead nuclei at TeV energies, matter and antimatter are abundantly produced in essentially equal amounts [37,53,56,115–120]. This fact not only facilitates detailed studies of (anti)nuclei production mechanisms [74,82], but also allows one to investigate the antinuclei inelastic interactions with the detector material. Last year, the ALICE Collaboration presented novel results of $\sigma_{\rm inel}^{\bar{\rm d}}$ in the momentum range below 4 GeV/c [65]. The analysis exploited the antimatter-to-matter ratio method, in which the raw reconstructed antideuteron-to-deuteron ratio ($\bar{\rm d}$/d) served as an experimental observable, as it is sensitive to the inelastic cross section of the (anti)nuclei entering the ratio. Since $\sigma_{\rm inel}({\rm d})$ at low energies is known [121,122], the antideuteron inelastic cross section $\sigma_{\rm inel}^{\bar{\rm d}}$ could be extracted by comparing the experimental results for raw reconstructed $\bar{\rm d}$/d with Monte Carlo simulations in which $\sigma_{\rm inel}({\rm d})$ is constrained by the available data. The resulting $\sigma_{\rm inel}^{\bar{\rm d}}$ is shown for the atomic mass numbers of $\langle A\rangle = 17.4$ and 31.8 in Fig. 4. These values of $\langle A\rangle$ were obtained by weighting the contribution from different materials of the ALICE detector with their density times the path length crossed by particles.

The results from ALICE are in good agreement within uncertainties with the parametrizations of $\sigma_{\rm inel}^{\bar{\rm d}}$ implemented in the GEANT4 toolkit [123], which is widely used for the propagation of particles through the matter. In this toolkit the description of antinucleus-nucleus inelastic cross sections is based on Glauber calculations. Direct Glauber model simulations during each propagation step in GEANT4 would be computationally too expensive, so the antinuclei inelastic cross sections are parametrized as a function of atomic mass number A of the target nucleus as described in [124]:

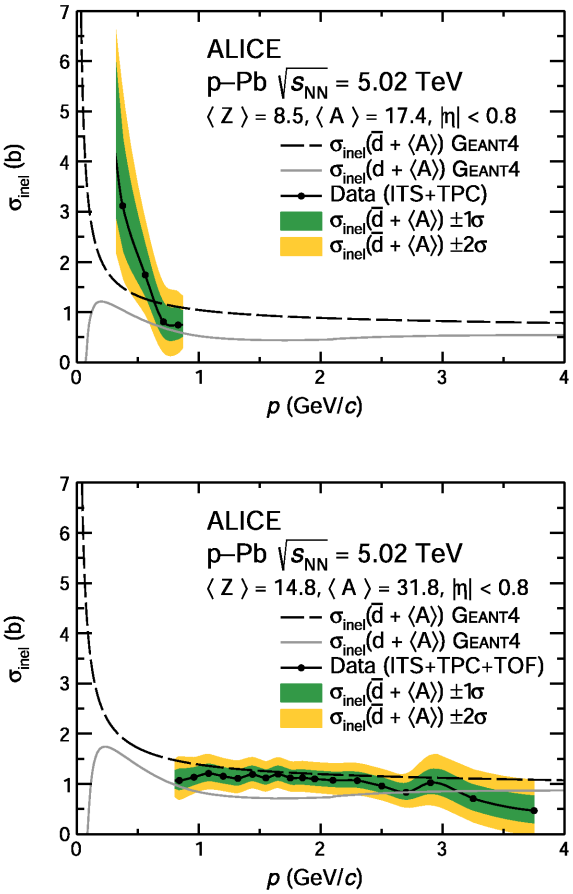

FIG. 4. $\sigma_{\rm inel}^{\bar{\rm d}}$ measured on an average material element of the ALICE detector as a function of the momentum [65]. Dashed black lines and full gray lines represent the GEANT4 parametrizations for $\sigma_{\rm inel}^{\bar{\rm d}}$ and $\sigma_{\rm inel}({\rm d})$, respectively. The experimental data points are connected by solid black lines, and green and orange bands correspond to ± 1 and $\pm 2\sigma$ uncertainties on $\sigma_{\rm inel}^{\bar{\rm d}}$.

$$\sigma_{hA}^{\rm inel} = \pi R_A^2 \ln\left(1 + \frac{A\sigma_{hN}^{\rm tot}}{\pi R_A^2}\right). \tag{7}$$

Here the total (elastic plus inelastic) cross section $\sigma_{hN}^{\rm tot}$ of a hadron h ($h = \bar{p}$, $\bar{d}$, $^3\overline{\rm He}$, or $^4\overline{\rm He}$) interacting with a nucleon N is estimated with Glauber calculations. A is the atomic number of the target nucleus with radius R_A, which is parametrized as a function of A using $\sigma_{hA}^{\rm inel}$ and $\sigma_{hN}^{\rm tot}$ calculated using the Glauber model for given h and A.

An alternative parametrization of $\sigma_{\rm inel}^{\bar{\rm d}}$ can be obtained from the total deuteron-antiproton cross section $\sigma_{\rm tot}^{\rm d\bar{p}}$ measured in [125]. By symmetry, it is equal to the total antideuteron-proton cross section $\sigma_{\rm tot}^{\bar{\rm d}{\rm p}}$ which, together with the known total and elastic antiproton-proton cross

sections [125], can be used to estimate the inelastic antideuteron-proton cross section in the following way:

$$\sigma_{\mathrm{inel}}^{\bar{\mathrm{d}}\mathrm{p}} \approx \frac{\sigma_{\mathrm{tot}}^{\bar{\mathrm{d}}\mathrm{p}}}{\sigma_{\mathrm{tot}}^{\bar{\mathrm{p}}\mathrm{p}}}(\sigma_{\mathrm{tot}}^{\bar{\mathrm{p}}\mathrm{p}} - \sigma_{\mathrm{el}}^{\bar{\mathrm{p}}\mathrm{p}}). \tag{8}$$

This approach has been used in previous studies estimating the antideuteron fluxes near Earth [16].

Another assumption which can be employed to estimate the antideuteron inelastic cross section is that it is simply twice as large as the corresponding antiproton inelastic cross section at the same kinetic energy per nucleon $E_{\mathrm{kin}}^{\bar{\mathrm{p}}} = E_{\mathrm{kin}}^{\bar{\mathrm{d}}}/n$ [10,12]:

$$\sigma_{\mathrm{inel}}^{\bar{\mathrm{d}}\mathrm{p}}(E_{\mathrm{kin}}^{\bar{\mathrm{d}}}/n) \approx 2\sigma_{\mathrm{inel}}^{\bar{\mathrm{p}}\mathrm{p}}(E_{\mathrm{kin}}^{\bar{\mathrm{p}}}). \tag{9}$$

The inelastic antiproton-proton cross section can be taken, e.g., from [126] as

$$\sigma_{\mathrm{inel}}^{\bar{\mathrm{p}}\mathrm{p}}(E_{\mathrm{kin}}^{\bar{\mathrm{p}}}) = 24.7(1 + 0.584 E_{\mathrm{kin}}^{\bar{\mathrm{p}}\ -0.115} \tag{10}$$

$$+ 0.856 E_{\mathrm{kin}}^{\bar{\mathrm{p}}\ -0.566}) \text{ mbarn}, \tag{11}$$

where $E_{\mathrm{kin}}^{\bar{\mathrm{p}}}$ is in units of GeV. For the inelastic cross section of antideuterons colliding with helium nuclei, the $\sigma_{\mathrm{inel}}^{\bar{\mathrm{d}}\mathrm{p}}$ can be scaled by the geometrical factor of $4^{2/3}$. The described approach has been used in antideuteron cosmic-ray studies presented in [12].

Unlike previous estimates, the results presented in the current paper are based entirely on experimental data for $\sigma_{\mathrm{inel}}^{\bar{\mathrm{d}}}$. In order to model the inelastic processes of antideuterons with matter, the results published in [65,113,114] are used to obtain a momentum-dependent correction factor for the $\sigma_{\mathrm{inel}}^{\bar{\mathrm{d}}}$ parametrization implemented in GEANT4. Figure 5 shows this correction factor as a function of the antideuteron momentum. The experimental data and their uncertainties from [65,113,114] are described with smooth functions using a combination of exponential and polynomial functions in order to interpolate the results into the momentum ranges with no measurements. The last two data points from [65] at p/nucleon $\lesssim 2$ GeV/c have been excluded from the fit to obtain a smooth interpolation between the results from ALICE and from U-70 experiments. For the extrapolation to momenta above the measured momentum range, the correction factor corresponding to the last measured value from [114] (at p/nucleon $= 12.5$ GeV/c) has been considered. The numerical values of the correction factor for $\sigma_{\mathrm{inel}}^{\bar{\mathrm{d}}}$ in GEANT4 can be found in Table II.

The resulting correction factor is applied to $\sigma_{\mathrm{inel}}^{\bar{\mathrm{d}}}$ from GEANT4 on all target materials relevant to our studies (mainly hydrogen and helium). Since the experimental data are only available for relatively heavy target elements

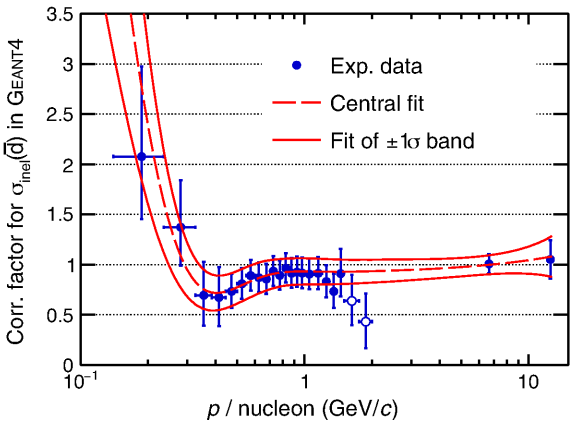

FIG. 5. Correction factor for $\sigma_{\mathrm{inel}}^{\bar{\mathrm{d}}}$ in GEANT4 as a function of the antideuteron momentum per nucleon. The correction factor obtained from experimental data [65,113,114] is shown as blue points, and red lines show the smooth fit used to describe the data. Two data points excluded from the fit are shown as open circles. The numerical values for the correction factor can be found in Table II.

TABLE II. Correction factor for $\sigma_{\mathrm{inel}}^{\bar{\mathrm{d}}}$ implemented in GEANT4. Data points enclosed in brackets have not been used for the fit.

Antideuteron momentum per nucleon, GeV/c	Correction factor for $\sigma_{\mathrm{inel}}^{\bar{\mathrm{d}}}$
0.1875 ± 0.0475	$2.076^{+0.897}_{-0.622}$
0.28 ± 0.045	$1.373^{+0.470}_{-0.381}$
0.355 ± 0.03	$0.694^{+0.332}_{-0.301}$
0.415 ± 0.03	$0.674^{+0.303}_{-0.287}$
0.4725 ± 0.0275	$0.735^{+0.175}_{-0.165}$
0.525 ± 0.025	$0.809^{+0.156}_{-0.149}$
0.575 ± 0.025	$0.890^{+0.156}_{-0.150}$
0.625 ± 0.025	$0.870^{+0.151}_{-0.145}$
0.675 ± 0.025	$0.856^{+0.153}_{-0.146}$
0.725 ± 0.025	$0.935^{+0.150}_{-0.144}$
0.775 ± 0.025	$0.893^{+0.148}_{-0.142}$
0.825 ± 0.025	$0.965^{+0.150}_{-0.145}$
0.875 ± 0.025	$0.914^{+0.150}_{-0.145}$
0.925 ± 0.025	$0.925^{+0.153}_{-0.147}$
0.975 ± 0.025	$0.916^{+0.154}_{-0.148}$
1.05 ± 0.05	$0.906^{+0.157}_{-0.152}$
1.15 ± 0.05	$0.914^{+0.163}_{-0.156}$
1.25 ± 0.05	$0.832^{+0.162}_{-0.156}$
1.35 ± 0.05	$0.733^{+0.173}_{-0.166}$
1.45 ± 0.05	$0.911^{+0.244}_{-0.229}$
(1.625 ± 0.125)	$(0.639^{+0.261}_{-0.244})$
(1.875 ± 0.125)	$(0.431^{+0.281}_{-0.262})$
6.65	1.0075 ± 0.0950
12.5	1.052 ± 0.193

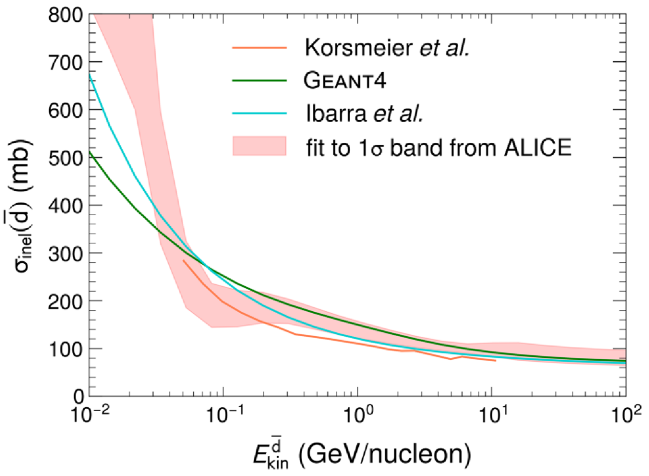

FIG. 6. Antideuteron-proton inelastic cross section as a function of kinetic energy per nucleon. The light red band shows the fit to available experimental data (see text for details), the dark green line represents the parametrization implemented in GEANT4, the orange line shows the parametrization employed in [16], and the turquoise line corresponds to the parametrization used in [12].

(e.g., $\langle A\rangle = 17.4$ and $\langle A\rangle = 34.7$ in the case of ALICE results), an additional uncertainty has been assigned to the fit results to take into account a possible dependence of this correction factor on the atomic mass number of target A. This uncertainty is taken from the difference between the parametrization for the A dependence implemented in GEANT4 and the full Glauber calculation and amounts to $< 8\%$ [124]. It is worth to mention that GEANT4 parametrizations describe well the antiproton inelastic cross section on various materials [124]. Therefore the deviations of the correction factor from unity seen in Fig. 5 are apparently related to the properties of antideuteron and not of the target, i.e., one should expect a weak dependence of this correction factor on A.

The resulting antideuteron-proton inelastic cross section is shown in Fig. 6 together with the parametrization used in GEANT4 and with the models employed in [12,16].

V. RESULTS

This section presents predictions for antideuteron fluxes calculated for observations near Earth from the sources discussed in Sec. III. In addition it highlights the different uncertainties—well quantified and qualitative ones—entering the calculation and discusses their importance.

The various antideuteron source functions described in Sec. III were implemented in the GALPROP cosmic-ray propagation code and the inelastic cross sections described in Sec. IV were also included in the GALPROP transport equation [see Eq. (1)]. The propagation parameters considered as a default have been taken from [72] and systematic studies of the impact of a different implementation of these parameters have been carried out, also considering the work of [31]. The effect of solar modulation is modeled employing the force-field approximation with constant Fisk potential $\phi = 0.5$ GV corresponding to solar minimum. The fluxes are shown after solar modulation only in Fig. 7.

A. Cosmic-ray fluxes

The predicted antideuteron fluxes at Earth for different sources are shown in Fig. 7, using fiducial values for source and propagation parameters. The horizontal black line shows the upper limit for the antideuteron flux obtained by the BESS experiment [1]. All panels show the secondary antideuteron flux produced in the collisions of cosmic rays in the interstellar medium. For secondary antideuterons, two coalescence models are considered: Shukla *et al.* [84] (red) and Kachelrieß *et al.* [63] (orange). The upper two panels of Fig. 7 show antideuterons from dark-matter annihilation into $b\bar{b}$ (left) and W^+W^- (right) for several dark-matter masses, using antideuteron spectra determined by [12]. The lower left panel shows the antideuteron fluxes obtained using production cross sections from Winkler *et al.* [104] for the $\bar{\Lambda}_b$ decay assumption as explained in Sec. III C. The lower right panel includes the antideuteron flux from primordial black hole evaporation. The solid lines were obtained using default GEANT4 parametrization values for both the dark-matter and cosmic-ray induced fluxes. The shaded bands were obtained with inelastic cross sections estimated using ALICE measurement as described in Sec. IV. This effect is discussed in the next Sec. V B 1 and translates into a small flux variation in comparison with the other unknowns entering the calculation.

Figure 7 leads to the well-known conclusion that low-energy antideuterons ($E_{kin} \leq 1$ GeV/nucleon) can exhibit a large signal-to-background ratio between exotic sources of antinuclei and secondary antideuterons. This holds independently of the coalescence model used for the secondary antideuteron flux for both GeV-scale annihilating dark matter and primordial black hole evaporation.

In the following, the different uncertainties entering the calculation of these fluxes are discussed, taking account of how well they are characterized and their relative importance in predicting the antideuteron flux.

B. Discussion of uncertainties

The limited knowledge of antideuteron production and propagation hampers the precise prediction of the local antideuteron flux. Equally important as the fiducial fluxes shown in Fig. 7 is the accounting for and discussion of the relevant uncertainties: the uncertainty due to inelastic scattering during propagation is quantified for the first time in Sec. V B 1. This experimental uncertainty is now several orders of magnitude smaller than the uncertainties due to antideuteron production (see Sec. V B 2) and diffusion in the Galactic magnetic field (Sec. V B 3), as

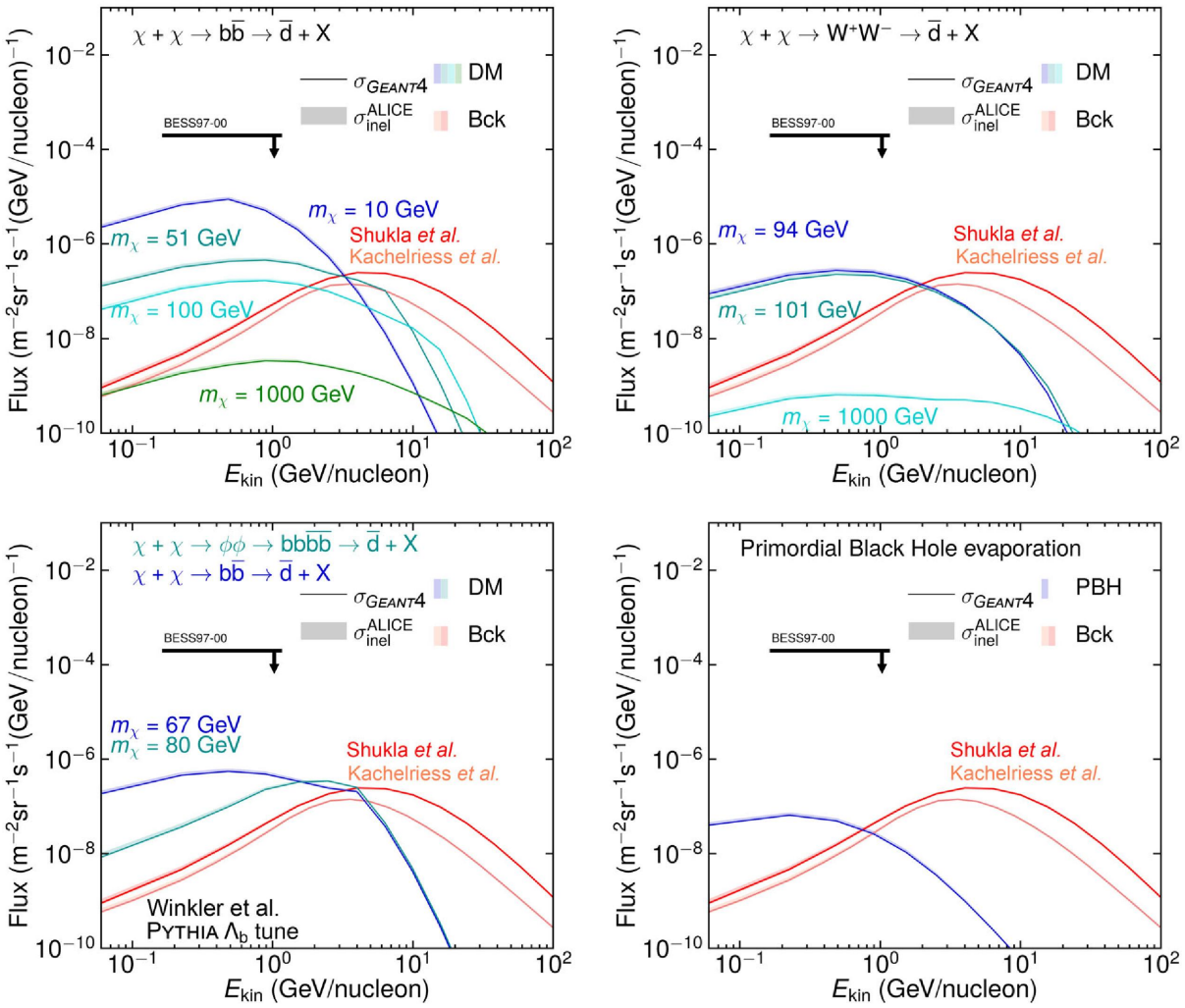

FIG. 7. Antideuteron fluxes from cosmic-ray collisions with the interstellar medium and for different production scenarios from dark-matter annihilation expected at Earth. Only uncertainties accounting for the inelastic cross section $\sigma^{\bar{d}}_{inel}$ are shown.

well as additional unknowns related to exotic sources of cosmic antideuterons (Sec. V B 4). All figures in this subsection show the local interstellar fluxes.

1. Loss of antideuteron flux via inelastic interactions

While the effect of inelastic losses during propagation on the final spectra is modest, it is essential to emphasize that the related uncertainty is now well quantified based on experimental data. The result for the inelastic antideuteron scattering cross section presented in Sec. IV is not radically different from previous determinations in terms of magnitude, but for the first time allows us properly to quantify the uncertainty in antideuteron flux predictions from inelastic losses. The effect of inelastic processes that cause the disappearance of antideuterons on the total flux near Earth for the two different sources is shown in the upper panels of Fig. 8. The left and right upper panels show the expected flux for secondary antideuterons and antideuterons from dark-matter annihilations considering a mass $m_\chi = 1000$ GeV for different assumptions on the inelastic interactions, respectively. The assumptions are as follows: no inelastic interactions at all (dashed lines) and different parametrizations of inelastic antideuteron cross sections taken from GEANT4 (solid line), from [12] (dot-dashed lines), from [16] (long-dashed lines) and considering the available experimental measurements [65,113,114] (colored bands). Details of the different parametrizations are described in Sec. IV.

One can see that fluxes calculated using the measured inelastic cross sections agree with previous parametrizations obtained from a scaling of the measured antiproton inelastic cross sections within the estimated uncertainties. Furthermore, the effect of the absorption on the calculated fluxes is most prominent at lower kinetic energies where the inelastic cross section is maximal (see Fig. 6). The uncertainty on the inelastic cross section does not translate linearly to the uncertainty on fluxes, as can be seen in the lower panels of Fig. 8, where this relative uncertainty is shown as a function of the antideuteron kinetic energy for

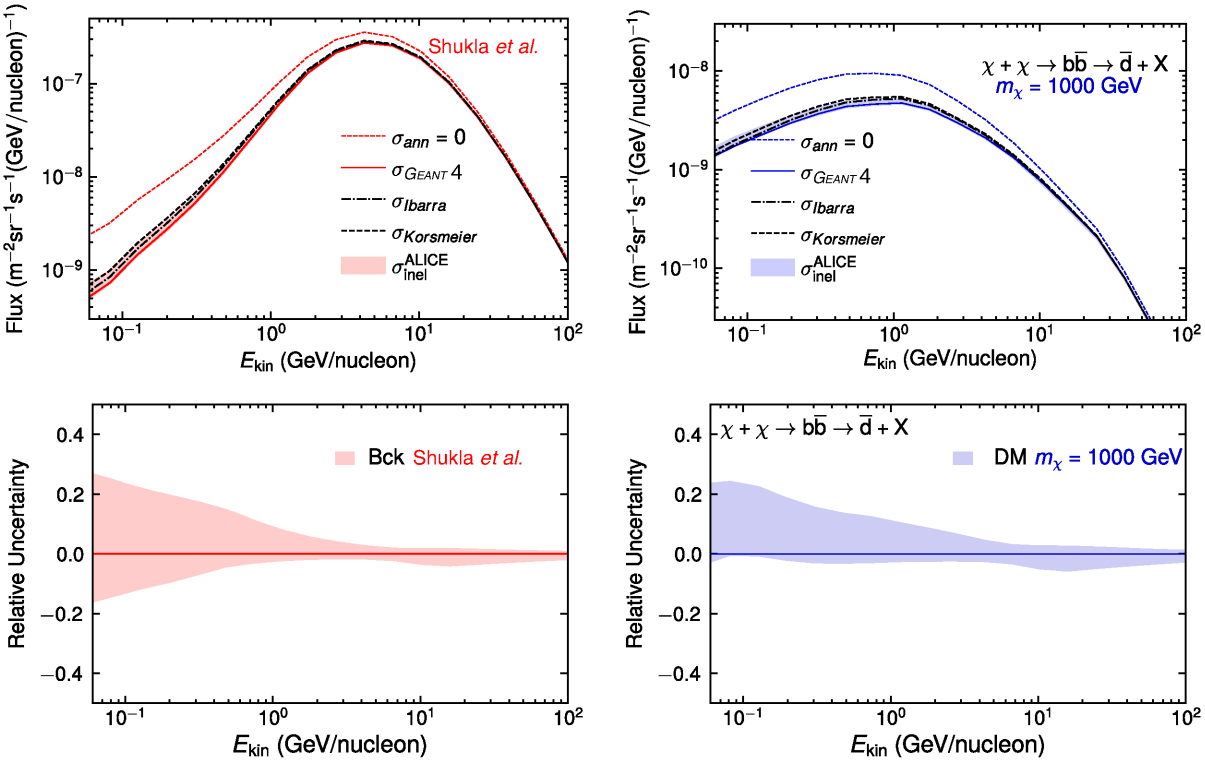

FIG. 8. Obtained fluxes for exemplary secondary and dark-matter models (top panels) and relative uncertainties obtained using data-driven estimates (bottom panels). The relative uncertainty is shown only from inelastic cross section and before solar modulation.

the secondary (left lower panel) and dark-matter sources (right lower panel). In general, the effect of inelastic scattering becomes stronger for longer propagation times. It is small at large energies, where cosmic-ray propagation is mainly escape dominated and larger at small energies. This holds in particular for secondary antideuterons, where energy losses are responsible for the reduction in flux below the production threshold.

2. Production uncertainty

The dominant uncertainty in predicting the antideuteron flux is related to our imperfect knowledge of antideuteron production in high-energy processes, see Sec. III A. Within a given coalescence model, the model parameters (the coalescence momentum p_0 in [61,84] and the size of emission region σ in [63]) are determined from fitting to antideuteron production data, and their plausible ranges can be determined. For secondary antideuterons, this is shown as red and orange bands in Fig. 7. The effect of adopting a smaller or larger coalescence momentum on the antideuteron yield is roughly independent of energy. This can be understood in terms of the separation of scales, where changing the coalescence condition at small energies does not significantly impact the overall energy distribution of the antinucleon pairs produced at higher energy. The quantified coalescence uncertainty hence amounts to a simple rescaling of the fluxes displayed in Fig. 7. For secondary antideuterons, this can be determined from data on antideuteron production in collisions of nuclei, resulting in $^{+27}_{-42}\%$ uncertainty on the flux for Shukla *et al.* [84], and $\pm 20\%$ for Kachelrieß *et al.* [63]. As there are no experimental data on the hypothetical processes of dark-matter annihilation or PBH evaporation, the situation is less clear in this case. The p_0 ranges required to reproduce antideuteron production at different Standard Model processes thought to most closely resemble dark-matter annihilation, or PBH evaporation (i.e., hard processes producing $\bar{q}q$ pairs in isolation) do not agree with each other. Taking their envelope, one obtains a plausible range of $^{+63}_{-70}\%$ for the dark-matter annihilation and PBH evaporation fluxes following [12], which can, however, no longer be interpreted as a meaningful uncertainty band.

More important than the uncertainty resulting from the determination of coalescence parameters within any given model may be the systematic uncertainty from imperfect modeling. For the secondary flux, this is evident in Fig. 2, where the two different secondary predictions often do not overlap within their uncertainty bands, with the estimated upper limit from the Shukla *et al.* model being up to seven times larger than the lower limit obtained employing the Kachelrieß *et al.* model. The same is true for exotic sources of antideuterons, where, in particular, there has been discussion regarding the possibility of increased antinuclei production in $\bar{\Lambda}_b$ decay [64,104,105]. Therefore, the

microscopic modeling of antideuteron production needs to be improved to reduce the current uncertainties, which requires measuring antideuteron production with accelerator experiments at different energies in different production channels. This scheme should be tuned for collisions at intermediate energies that match the energy scale of the processes induced by cosmic rays. The studies of the antinuclei formation arising from charm-hadron decays could help in better constraining possible dark-matter decays.

3. Propagation parameters

Propagation models are constrained by measurements of several primary and secondary cosmic-ray species. The parameters obtained by Boschini *et al.* were used as defaults in this work. We also compute fluxes using parameters by Cuoco *et al.* [29] to illustrate the uncertainty related to propagation. Both sets of propagation parameters are summarized in Table I. Boschini *et al.* used Voyager 1, AMS-02, HEAO-3-C2, and ACE-CRIS experimental data to fit the propagation parameters [72] while Cuoco *et al.* employed Voyager 1, AMS-02, and CREAM data [29].

Figure 9 compares antideuteron fluxes obtained with these two propagation benchmarks. While propagation parameters in the two works are rather different, the computed fluxes of secondary antideuterons at higher energies ($E_{\rm kin} \geq 1$ GeV/nucleon) are in good agreement (see upper panel of Fig. 9). This is expected since both benchmarks were built to reproduce the available AMS-02 data, which constrains this energy regime very well. The difference at low energies can be attributed to the stronger convection effects assumed by Cuoco *et al.*

In the case of the antideuteron flux arising from dark-matter annihilation (see lower panel of Fig. 9), the flux obtained using the propagation parameters from Cuoco *et al.* is about 2–3 times larger at all energies than that using the Boschini *et al.* parameters. This can be explained by the different halo half-width values in the parametrizations ($z_{\rm h}$ parameter in Table I). It is well known that there is a degeneracy between the height of the diffusive halo and the diffusion coefficient when predicting secondary cosmic-ray fluxes. However the dark-matter halo extends well beyond the diffusive halo, and the larger diffusive halo results in a larger number of diffusively confined dark-matter annihilation products. This enhancement of the dark-matter induced antideuteron flux with larger halo size does not depend strongly on energy and is the same for antiprotons and antideuterons. Hence, the associated uncertainty largely cancels when predicting antideuteron fluxes based on antiproton signals or limits.

4. Dark-matter specific uncertainties

The possible antideuteron flux arising from dark-matter annihilation is not well constrained since knowledge of the hypothetical dark-matter particles is very limited. For example, the dark-matter mass $m_{\rm DM}$ is not known. For the velocity-averaged annihilation cross section $\langle\sigma v\rangle$, there is the well-motivated thermal WIMP benchmark value $\langle\sigma v\rangle_{\rm thermal}$, from which it can differ by orders of magnitude. This can be both due to effects particular to any given WIMP model (e.g., velocity suppressed annihilation cross section, Sommerfeld enhancement) or astrophysical boost factors due to dark-matter clumping (e.g., [127]). Still, results for different dark-matter masses and annihilation channels together give a qualitative picture of what kind of

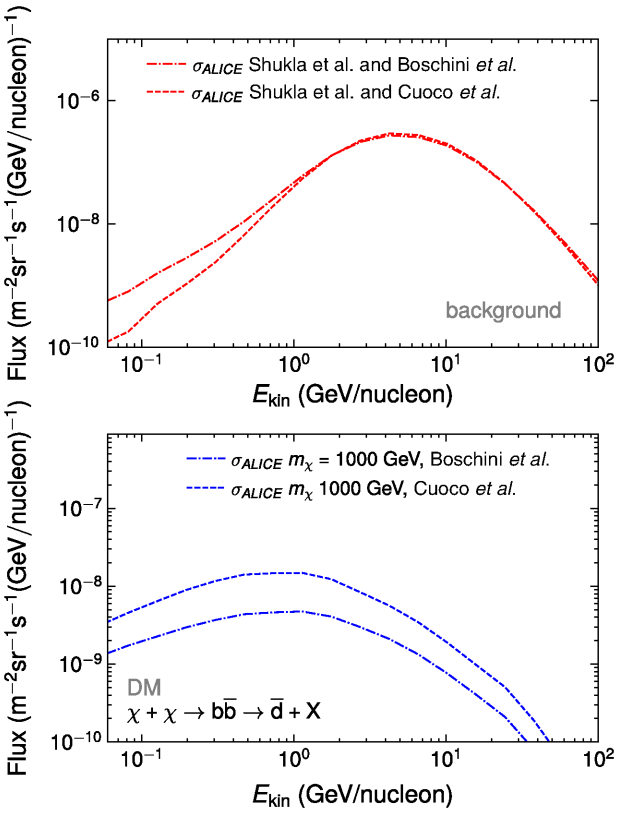

FIG. 9. The antideuteron flux obtained using two different sets of propagation parameters.

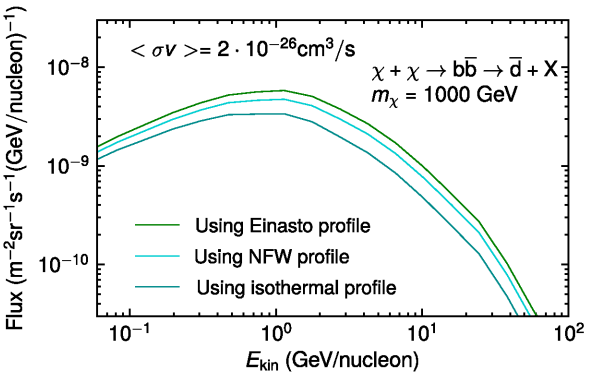

FIG. 10. Antideuteron fluxes from dark-matter annihilations for different dark-matter density profiles.

dark-matter-induced antideuteron fluxes can be expected (cf. Fig. 7). The uncertainty arising from the choice of the dark-matter density profile is shown in Fig. 10. The isothermal profile shown in Fig. 3 assumes a smaller density of dark matter in the inner Galaxy than the NFW profile and thus results in 14%–62% smaller antideuteron fluxes, as seen in Fig. 10. On the other hand, as the Einasto profile assumes a higher central density of dark matter than NFW, it results in 12%–44% higher fluxes. As can be seen in Fig. 10, the resulting difference is largely a normalization effect. Such normalization uncertainties shared by antiprotons and antideuterons from DM cancel exactly when predicting antideuteron fluxes based on antiproton signals or limits.

VI. SUMMARY

In summary, updated antideuteron fluxes at Earth for several dark-matter masses and two models for the secondary production due to cosmic rays have been presented, taking into account for the first time the measurement of the antideuteron inelastic cross section. The error associated with this measurement is propagated to the antideuteron flux and we show that because of the new experimental measurement this component of the modeling is very well constrained and has negligible uncertainty with respect to the other uncertainty sources.

The results have been evaluated following a consistent scheme, in which all fluxes are obtained using the same propagation model and the same inelastic cross section. Thus it is possible to compare the two considered models for the secondary sources quantitatively. A detailed discussion of the uncertainties related to the predicted fluxes show that the major contributions are currently associated to propagation parameters, to the microscopic modeling of antinuclei formations in both cosmic-rays collisions and dark-matter decays and to the still unconstrained dark-matter modeling.

The current work represents a state-of-the-art method for antideuteron predictions that could be further advanced only by improving the experimental studies of light nuclei formation and their interpretation, to be applied to both dark matter and secondary sources, and on the extension of the kinematic range for the inelastic cross section measurements. The microscopic behavior of nuclei production should especially be understood in the energy range most relevant for the astrophysical processes.

The potential of antideuterons as a messenger is not changed by this work. While the effect of inelastic losses during propagation on the final spectra is modest, it should be emphasized that the related uncertainty is now well quantified based on experimental data. Further studies at accelerator will help in improving the predictions and interpreting future antideuteron signals by satellite or balloon experiments.

ACKNOWLEDGMENTS

We are grateful to M. Kachelrieß and J. Tjemsland for providing us with their antideuteron production cross sections. We thank as well M. Winkler for providing us the antideuteron spectra from dark matter annihilation. P. von Doetinchem, D. Gomez, and A. Shukla received support from the National Science Foundation under Grant No. PHY-2013228. This research was done using resources provided by the Open Science Grid, which is supported by the National Science Foundation Grant No. 1148698, and the U.S. Department of Energy's Office of Science. The technical support and advanced computing resources from University of Hawaii Information Technology Services—Cyberinfrastructure, funded in part by the National Science Foundation MRI Grant No. 1920304, are gratefully acknowledged. This work is supported by the Deutsche Forschungsgemeinschaft (DFG, German Research Foundation) through Grant SFB 1258 "Neutrinos and Dark Matter in Astro- and Particle Physics" and through Excellence Cluster ORIGINS under Germany's Excellence Strategy-EXC-2094-390783311.

[1] H. Fuke, T. Maeno, K. Abe, S. Haino, Y. Makida, S. Matsuda, H. Matsumoto, J. W. Mitchell, A. A. Moiseev, J. Nishimura *et al.*, Search for Cosmic-Ray Antideuterons, Phys. Rev. Lett. **95**, 081101 (2005).

[2] K. Abe, H. Fuke, S. Haino, T. Hams, M. Hasegawa, A. Horikoshi, A. Itazaki, K. C. Kim, T. Kumazawa, A. Kusumoto *et al.*, Search for Antihelium with the BESS-Polar Spectrometer, Phys. Rev. Lett. **108**, 131301 (2012).

[3] K. Abe, H. Fuke, S. Haino, T. Hams, M. Hasegawa, A. Horikoshi, K. C. Kim, A. Kusumoto, M. H. Lee, Y. Makida *et al.*, Measurement of the Cosmic-Ray Antiproton Spectrum at Solar Minimum with a Long-Duration Balloon Flight over Antarctica, Phys. Rev. Lett. **108**, 051102 (2012).

[4] O. Adriani, G. A. Bazilevskaya, G. C. Barbarino, R. Bellotti, M. Boezio, E. A. Bogomolov, V. Bonvicini, M. Bongi, L. Bonechi, S. V. Borisov *et al.*, Measurement of the flux of primary cosmic ray antiprotons with energies of 60 MeV to 350 GeV in the PAMELA experiment, Sov. J. Exp. Theor. Phys. Lett. **96**, 621 (2013).

[5] O. Adriani *et al.* (PAMELA Collaboration), Ten years of PAMELA in space, Riv. Nuovo Cimento **40**, 473 (2017).

[6] A. W. Strong and I. V. Moskalenko, Propagation of cosmic-ray nucleons in the galaxy, Astrophys. J. **509**, 212 (1998).
[7] M. Aguilar *et al.* (AMS Collaboration), Antiproton Flux, Antiproton-to-Proton Flux Ratio, and Properties of Elementary Particle Fluxes in Primary Cosmic Rays Measured with the Alpha Magnetic Spectrometer on the International Space Station, Phys. Rev. Lett. **117**, 091103 (2016).
[8] F. Donato, N. Fornengo, and P. Salati, Antideuterons as a signature of supersymmetric dark matter, Phys. Rev. D **62**, 043003 (2000).
[9] H. Baer and S. Profumo, Low energy antideuterons: Shedding light on dark matter, J. Cosmol. Astropart. Phys. 12 (2005) 008.
[10] F. Donato, N. Fornengo, and D. Maurin, Antideuteron fluxes from dark matter annihilation in diffusion models, Phys. Rev. D **78**, 043506 (2008).
[11] R. Duperray, B. Baret, D. Maurin, G. Boudoul, A. Barrau, L. Derome, K. Protasov, and M. Buenerd, Flux of light antimatter nuclei near Earth, induced by cosmic rays in the Galaxy and in the atmosphere, Phys. Rev. D **71**, 083013 (2005).
[12] A. Ibarra and S. Wild, Prospects of antideuteron detection from dark matter annihilations or decays at AMS-02 and GAPS, J. Cosmol. Astropart. Phys. 02 (2013) 021.
[13] A. Ibarra and S. Wild, Determination of the cosmic antideuteron flux in a Monte Carlo approach, Phys. Rev. D **88**, 023014 (2013).
[14] N. Fornengo, L. Maccione, and A. Vittino, Dark matter searches with cosmic antideuterons: Status and perspectives, J. Cosmol. Astropart. Phys. 09 (2013) 031.
[15] L. Dal and A. Raklev, Antideuteron limits on decaying dark matter with a tuned formation model, Phys. Rev. D **89**, 103504 (2014).
[16] M. Korsmeier, F. Donato, and N. Fornengo, Prospects to verify a possible dark matter hint in cosmic antiprotons with antideuterons and antihelium, Phys. Rev. D **97**, 103011 (2018).
[17] N. Tomassetti and A. Oliva, Production of cosmic-ray antinuclei in the Galaxy and background for dark matter searches, in Proceedings of the 2017 European Physical Society Conference on High Energy Physics (EPS-HEP 2017): Venice, Italy, 2017 [*Proc. Sci.*, EPS-HEP2017 (2017) 620].
[18] S.-J. Lin, X.-J. Bi, and P.-F. Yin, Expectations of the cosmic antideuteron flux, arXiv:1801.00997.
[19] Y.-C. Ding, N. Li, C.-C. Wei, Y.-L. Wu, and Y.-F. Zhou, Prospects of detecting dark matter through cosmic-ray antihelium with the antiproton constraints, J. Cosmol. Astropart. Phys. 06 (2019) 004.
[20] M. Cirelli, N. Fornengo, M. Taoso, and A. Vittino, Antihelium from Dark Matter annihilations, J. High Energy Phys. 08 (2014) 009.
[21] E. Carlson, A. Coogan, T. Linden, S. Profumo, A. Ibarra, and S. Wild, Antihelium from dark matter, Phys. Rev. D **89**, 076005 (2014).
[22] A. Coogan and S. Profumo, Origin of the tentative AMS antihelium events, Phys. Rev. D **96**, 083020 (2017).
[23] O. Adriani *et al.* (PAMELA Collaboration), An anomalous positron abundance in cosmic rays with energies 1.5–100 GeV, Nature (London) **458**, 607 (2009).
[24] M. Aguilar *et al.* (AMS Collaboration), First Result from the Alpha Magnetic Spectrometer on the International Space Station: Precision Measurement of the Positron Fraction in Primary Cosmic Rays of 0.5–350 GeV, Phys. Rev. Lett. **110**, 141102 (2013).
[25] L. Accardo *et al.* (AMS Collaboration), High Statistics Measurement of the Positron Fraction in Primary Cosmic Rays of 0.5–500 GeV with the Alpha Magnetic Spectrometer on the International Space Station, Phys. Rev. Lett. **113**, 121101 (2014).
[26] I. V. Moskalenko and A. W. Strong, Production and propagation of cosmic-ray positrons and electrons, Astrophys. J. **493**, 694 (1998).
[27] M. Boudaud, S. Aupetit, S. Caroff, A. Putze, G. Belanger, Y. Genolini, C. Goy, V. Poireau, V. Poulin, S. Rosier *et al.*, A new look at the cosmic ray positron fraction, Astron. Astrophys. **575**, A67 (2015).
[28] M.-Y. Cui, Q. Yuan, Y.-L. S. Tsai, and Y.-Z. Fan, Possible Dark Matter Annihilation Signal in the AMS-02 Antiproton Data, Phys. Rev. Lett. **118**, 191101 (2017).
[29] A. Cuoco, M. Krämer, and M. Korsmeier, Novel Dark Matter Constraints from Antiprotons in Light of AMS-02, Phys. Rev. Lett. **118**, 191102 (2017).
[30] A. Reinert and M. W. Winkler, A precision search for WIMPs with charged cosmic rays, J. Cosmol. Astropart. Phys. 01 (2018) 055.
[31] A. Cuoco, J. Heisig, L. Klamt, M. Korsmeier, and M. Krämer, Scrutinizing the evidence for dark matter in cosmic-ray antiprotons, Phys. Rev. D **99**, 103014 (2019).
[32] I. Cholis, T. Linden, and D. Hooper, A robust excess in the cosmic-ray antiproton spectrum: Implications for annihilating dark matter, Phys. Rev. D **99**, 103026 (2019).
[33] M. Boudaud, Y. Génolini, L. Derome, J. Lavalle, D. Maurin, P. Salati, and P. D. Serpico, AMS-02 antiprotons' consistency with a secondary astrophysical origin, Phys. Rev. Research **2**, 023022 (2020).
[34] J. Heisig, M. Korsmeier, and M. W. Winkler, Dark matter or correlated errors: Systematics of the AMS-02 antiproton excess, Phys. Rev. Research **2**, 043017 (2020).
[35] T. Aramaki, S. Boggs, S. Bufalino, L. Dal, P. von Doetinchem, F. Donato, N. Fornengo, H. Fuke, M. Grefe, C. Hailey *et al.*, Review of the theoretical and experimental status of dark matter identification with cosmic-ray antideuterons, Phys. Rep. **618**, 1 (2016).
[36] P. von Doetinchem, K. Perez, T. Aramaki, S. Baker, S. Barwick, R. Bird, M. Boezio, S. Boggs, M. Cui, A. Datta *et al.*, Cosmic-ray antinuclei as messengers of new physics: Status and outlook for the new decade, J. Cosmol. Astropart. Phys. 08 (2020) 035.
[37] S. Acharya *et al.* (ALICE Collaboration), Production of deuterons, tritons, ^{3}He nuclei and their antinuclei in pp collisions at $\sqrt{s} = 0.9$, 2.76 and 7 TeV, Phys. Rev. C **97**, 024615 (2018).
[38] T. Aramaki, S. E. Boggs, P. von Doetinchem, H. Fuke, C. J. Hailey, S. A. I. Mognet, R. A. Ong, K. Perez, and J. Zweerink (GAPS Collaboration), Potential for precision measurement of low-energy antiprotons with GAPS for

dark matter and primordial black hole physics, Astropart. Phys. **59**, 12 (2014).
[39] T. Aramaki, C. J. Hailey, S. E. Boggs, P. von Doetinchem, H. Fuke, S. I. Mognet, R. A. Ong, K. Perez, and J. Zweerink (GAPS Collaboration), Antideuteron sensitivity for the GAPS experiment, Astropart. Phys. **74**, 6 (2016).
[40] N. Saffold *et al.* (GAPS Collaboration), Cosmic antihelium-3 nuclei sensitivity of the GAPS experiment, Astropart. Phys. **130**, 102580 (2021).
[41] A. Kounine (AMS Collaboration), The latest results from the alpha magnetic spectrometer, Proc. Sci., EPS-HEP2019 (**2020**) 028.
[42] J. Simon-Gillo *et al.* (NA44 Collaboration), Deuteron and anti-deuteron production in CERN experiment NA44, Nucl. Phys. **A590**, 483C (1995).
[43] T. Armstrong *et al.* (E864 Collaboration), Anti-Deuteron Yield at the AGS and Coalescence Implications, Phys. Rev. Lett. **85**, 2685 (2000).
[44] S. Afanasiev *et al.* (NA49 Collaboration), Deuteron production in central Pb + Pb collisions at 158-A-GeV, Phys. Lett. B **486**, 22 (2000).
[45] T. Anticic *et al.* (NA49 Collaboration), Energy and centrality dependence of deuteron and proton production in Pb + Pb collisions at relativistic energies, Phys. Rev. C **69**, 024902 (2004).
[46] S. Adler *et al.* (PHENIX Collaboration), Deuteron and Antideuteron Production in Au + Au Collisions at $\sqrt{s_{\mathrm{NN}}} = 200$-GeV, Phys. Rev. Lett. **94**, 122302 (2005).
[47] B. Alper, H. Bøggild, P. Booth, F. Bulos, L. Carroll, G. von Dardel, G. Damgaard, B. Duff, F. Heymann, J. Jackson *et al.*, Large angle production of stable particles heavier than the proton and a search for quarks at the cern intersecting storage rings, Phys. Lett. **46B**, 265 (1973).
[48] S. Henning *et al.* (British-Scandinavian-MIT Collaboration), Production of deuterons and anti-deuterons in proton proton collisions at the CERN ISR, Lett. Nuovo Cimento **21**, 189 (1978).
[49] T. Alexopoulos *et al.* (Fermilab E735 Collaboration), Cross sections for deuterium, tritium, and helium production in $\bar{p}p$ collisions at $\sqrt{s} = 1.8$ tev, Phys. Rev. D **62**, 072004 (2000).
[50] A. Aktas *et al.* (H1 Collaboration), Measurement of anti-deuteron photoproduction and a search for heavy stable charged particles at HERA, Eur. Phys. J. C **36**, 413 (2004).
[51] D. Asner *et al.* (CLEO Collaboration), Anti-deuteron production in Upsilon(nS) decays and the nearby continuum, Phys. Rev. D **75**, 012009 (2007).
[52] S. Schael *et al.* (ALEPH Collaboration), Deuteron and anti-deuteron production in e+ e- collisions at the Z resonance, Phys. Lett. B **639**, 192 (2006).
[53] J. Adam *et al.* (ALICE Collaboration), Production of light nuclei and anti-nuclei in pp and Pb-Pb collisions at energies available at the CERN large hadron collider, Phys. Rev. C **93**, 024917 (2016).
[54] J. Adam *et al.* (ALICE Collaboration), ${}^{3}_{\Lambda}\mathrm{H}$ and ${}^{3}_{\bar{\Lambda}}\bar{\mathrm{H}}$ production in Pb–Pb collisions at $\sqrt{s_{\mathrm{NN}}} = 2.76$ TeV, Phys. Lett. B **754**, 360 (2016).
[55] S. Acharya *et al.* (ALICE Collaboration), Measurement of deuteron spectra and elliptic flow in Pb–Pb collisions at $\sqrt{s_{\mathrm{NN}}} = 2.76$ TeV at the LHC, Eur. Phys. J. C **77**, 658 (2017).
[56] S. Acharya *et al.* (ALICE Collaboration), Multiplicity dependence of (anti-)deuteron production in pp collisions at $\sqrt{s} = 7$ TeV, Phys. Lett. B **794**, 50 (2019).
[57] H. Agakishiev *et al.* (STAR Collaboration), Observation of the antimatter helium-4 nucleus, Nature (London) **473**, 353 (2011).
[58] B. I. Abelev *et al.* (STAR Collaboration), Observation of an antimatter hypernucleus, Science **328**, 58 (2010).
[59] J. Adam *et al.* (ALICE Collaboration), Precision measurement of the mass difference between light nuclei and anti-nuclei, Nat. Phys. **11**, 811 (2015).
[60] J. Adam *et al.* (STAR Collaboration), Measurement of the mass difference and the binding energy of the hypertriton and antihypertriton, Nat. Phys. **16**, 409 (2020).
[61] D.-M. Gomez-Coral, A. Menchaca Rocha, V. Grabski, A. Datta, P. von Doetinchem, and A. Shukla, Deuteron and antideuteron production simulation in cosmic-ray interactions, Phys. Rev. D **98**, 023012 (2018).
[62] K. Blum and M. Takimoto, Nuclear coalescence from correlation functions, Phys. Rev. C **99**, 044913 (2019).
[63] M. Kachelrieß, S. Ostapchenko, and J. Tjemsland, Revisiting cosmic ray antinuclei fluxes with a new coalescence model, J. Cosmol. Astropart. Phys. 08 (2020) 048.
[64] M. W. Winkler and T. Linden, Response to comment on "Dark matter annihilation can produce a detectable antihelium flux through $\bar{\Lambda}_b$ decays", arXiv:2106.00053.
[65] S. Acharya *et al.* (ALICE Collaboration), Measurement of the Low-Energy Antideuteron Inelastic Cross Section, Phys. Rev. Lett. **125**, 162001 (2020).
[66] N. Abgrall *et al.* (NA61 Collaboration), NA61/SHINE facility at the CERN SPS: Beams and detector system, J. Instrum. **9**, P06005 (2014).
[67] A. W. Strong, I. V. Moskalenko, and V. S. Ptuskin, Cosmic-ray propagation and interactions in the Galaxy, Annu. Rev. Nucl. Part. Sci. **57**, 285 (2007).
[68] I. A. Grenier, J. H. Black, and A. W. Strong, The nine lives of cosmic rays in galaxies, Annu. Rev. Astron. Astrophys. **53**, 199 (2015).
[69] L. J. Gleeson and W. I. Axford, Solar modulation of galactic cosmic rays, Astrophys. J. **154**, 1011 (1968).
[70] M. Boschini, S. Della Torre, M. Gervasi, G. La Vacca, and P. Rancoita, Propagation of cosmic rays in heliosphere: The helmod model, Adv. Space Res. **62**, 2859 (2018).
[71] M. Boschini, S. Della Torre, M. Gervasi, G. La Vacca, and P. Rancoita, The HelMod model in the works for inner and outer heliosphere: From AMS to voyager probes observations, Adv. Space Res. **64**, 2459 (2019).
[72] M. J. Boschini, S. Della Torre, M. Gervasi, D. Grandi, G. Jóhannesson, G. La Vacca, N. Masi, I. V. Moskalenko, S. Pensotti, T. A. Porter *et al.*, Inference of the local interstellar spectra of cosmic-ray nuclei $Z \leq 28$ with the GalProp-HelMod framework, Astrophys. J. Suppl. Ser. **250**, 27 (2020).
[73] G. Jóhannesson and T. A. Porter, Signatures of recent cosmic-ray acceleration in the high-latitude gamma-ray sky, Astrophys. J. **917**, 30 (2021).
[74] A. Andronic, P. Braun-Munzinger, J. Stachel, and H. Stocker, Production of light nuclei, hypernuclei and their

antiparticles in relativistic nuclear collisions, Phys. Lett. B **697**, 203 (2011).
[75] P. Braun-Munzinger and B. Dönigus, Loosely-bound objects produced in nuclear collisions at the LHC, Nucl. Phys. **A987**, 144 (2019).
[76] S. T. Butler and C. A. Pearson, Deuterons from high-energy proton bombardment of matter, Phys. Rev. **129**, 836 (1963).
[77] M. Kadastik, M. Raidal, and A. Strumia, Enhanced anti-deuteron Dark Matter signal and the implications of PAMELA, Phys. Lett. B **683**, 248 (2010).
[78] V. Poulin, P. Salati, I. Cholis, M. Kamionkowski, and J. Silk, Where do the AMS-02 antihelium events come from?, Phys. Rev. D **99**, 023016 (2019).
[79] S. Acharya *et al.* (ALICE Collaboration), Production of deuterons, tritons, ^{3}He nuclei, and their antinuclei in pp collisions at $\sqrt{s} = 0.9$, 2.76, and 7 tev, Phys. Rev. C **97**, 024615 (2018).
[80] F. Bellini and A. P. Kalweit, Testing production scenarios for (anti-)(hyper-)nuclei and exotica at energies available at the CERN large hadron collider, Phys. Rev. C **99**, 054905 (2019).
[81] S. Acharya *et al.* (ALICE Collaboration), Search for a common baryon source in high-multiplicity pp collisions at the LHC, Phys. Lett. B **811**, 135849 (2020).
[82] F. Bellini, K. Blum, A. P. Kalweit, and M. Puccio, Examination of coalescence as the origin of nuclei in hadronic collisions, Phys. Rev. C **103**, 014907 (2021).
[83] M. Kachelrieß, S. Ostapchenko, and J. Tjemsland, Alternative coalescence model for deuteron, tritium, helium-3 and their antinuclei, Eur. Phys. J. A **56**, 4 (2020).
[84] A. Shukla, A. Datta, P. von Doetinchem, D.-M. Gomez-Coral, and C. Kanitz, Large-scale simulations of antihelium production in cosmic-ray interactions, Phys. Rev. D **102**, 063004 (2020).
[85] T. Pierog, I. Karpenko, J. M. Katzy, E. Yatsenko, and K. Werner, EPOS LHC: Test of collective hadronization with data measured at the CERN large hadron collider, Phys. Rev. C **92**, 034906 (2015).
[86] V. Abramov *et al.*, Production of deuterons and antideuterons with large p_T in pp and pA collisions at 70 GeV, Sov. J. Nucl. Phys. **45**, 845 (1987), https://inspirehep.net/literature/230030.
[87] J. Herms, A. Ibarra, A. Vittino, and S. Wild, Antideuterons in cosmic rays: Sources and discovery potential, J. Cosmol. Astropart. Phys. 02 (2017) 018.
[88] T. Sjostrand, S. Mrenna, and P. Z. Skands, A brief introduction to PYTHIA8.1, Comput. Phys. Commun. **178**, 852 (2008).
[89] J. P. Lees *et al.* (*BABAR* Collaboration), Antideuteron production in $\Upsilon(nS)$ decays and in $e^+e^- \to q\bar{q}$ at $\sqrt{s} \approx 10.58$ GeV, Phys. Rev. D **89**, 111102 (2014).
[90] I. V. Moskalenko, A. W. Strong, J. F. Ormes, and M. S. Potgieter, Secondary anti-protons and propagation of cosmic rays in the galaxy and heliosphere, Astrophys. J. **565**, 280 (2002).
[91] T. Pierog, C. Baus, and R. Ulrich, CRMC (Cosmic Ray Monte Carlo package), web.ikp.kit.edu/rulrich/crmc.html.
[92] D. M. Gomez Coral, Deuteron and antideuteron production in galactic cosmic-rays. Producción de deuterio y antideuterio en rayos cósmicos galácticos, Ph.D. thesis, 2019, presented 26 April 2019.
[93] G. Bertone, D. Hooper, and J. Silk, Particle dark matter: Evidence, candidates and constraints, Phys. Rep. **405**, 279 (2005).
[94] P. F. de Salas and A. Widmark, Dark matter local density determination: recent observations and future prospects, Rep. Prog. Phys. **84**, 104901 (2021).
[95] J. F. Navarro, C. S. Frenk, and S. D. M. White, A universal density profile from hierarchical clustering, Astrophys. J. **490**, 493 (1997).
[96] K. G. Begeman, A. H. Broeils, and R. H. Sanders, Extended rotation curves of spiral galaxies: Dark haloes and modified dynamics, Mon. Not. R. Astron. Soc. **249**, 523 (1991).
[97] M. Benito, F. Iocco, and A. Cuoco, Uncertainties in the galactic dark matter distribution: An update, Phys. Dark Universe **32**, 100826 (2021).
[98] T. Bringmann, P. F. Depta, M. Hufnagel, and K. Schmidt-Hoberg, Precise dark matter relic abundance in decoupled sectors, Phys. Lett. B **817**, 136341 (2021).
[99] P. A. R. Ade *et al.* (Planck Collaboration), Planck 2015 results. XIII. Cosmological parameters, Astron. Astrophys. **594**, A13 (2016).
[100] K. Griest and M. Kamionkowski, Unitarity Limits on the Mass and Radius of Dark Matter Particles, Phys. Rev. Lett. **64**, 615 (1990).
[101] S. Ting, The First Five Years of the Alpha Magnetic Spectrometer on the International Space Station, Press Conference at CERN, December 8 (2016), https://indico.cern.ch/event/592392/attachments/1381599/2110332/AMS-CERN-Dec-2016.pdf.
[102] S. Ting, Latest Results from the AMS Experiment on the International Space Station, Colloquium at CERN, May 24 (2018), https://cds.cern.ch/record/2320166?ln=en.
[103] A. Kounine, AMS Experiment on the International Space Station, Next Generation of AstroParticle Experiments in Space (NextGAPES-2019) (2019).
[104] M. W. Winkler and T. Linden, Dark Matter Annihilation Can Produce a Detectable Antihelium Flux through $\bar{\Lambda}_b$ Decays, Phys. Rev. Lett. **126**, 101101 (2021).
[105] M. Kachelriess, S. Ostapchenko, and J. Tjemsland, Comment on "Dark matter annihilation can produce a detectable antihelium flux through $\bar{\lambda}_b$ decays", arXiv:2105.00799.
[106] M.-Y. Cui, X. Pan, Q. Yuan, Y.-Z. Fan, and H.-S. Zong, Revisit of cosmic ray antiprotons from dark matter annihilation with updated constraints on the background model from AMS-02 and collider data, J. Cosmol. Astropart. Phys. 06 (2018) 024.
[107] A. Albert *et al.*, Searching for dark matter annihilation in recently discovered Milky Way satellites with Fermi-LAT, Astrophys. J. **834**, 110 (2017).
[108] S. Hawking, Gravitationally collapsed objects of very low mass, Mon. Not. R. Astron. Soc. **152**, 75 (1971).
[109] Y. B. Zel'dovich and I. D. Novikov, The hypothesis of cores retarded during expansion and the hot cosmological model, Sov. Astron. **10**, 602 (1967).
[110] S. W. Hawking, Black hole explosions?, Nature (London) **248**, 30 (1974).
[111] S. W. Hawking, Particle creation by black holes, Commun. Math. Phys. **43**, 199 (1975).

[112] B. J. Carr, The primordial black hole mass spectrum, Astrophys. J. **201**, 1 (1975).

[113] S. Denisov, S. Donskov, Y. Gorin, V. Kachanov, V. Kutjin, A. Petrukhin, Y. Prokoshkin, E. Razuvaev, R. Shuvalov, and D. Stojanova, Measurements of anti-deuteron absorption and stripping cross sections at the momentum 13.3 GeV/c, Nucl. Phys. **B31**, 253 (1971).

[114] F. Binon, S. Denisov, S. Donskov, P. Duteil, G. Giacomelli, Y. Gorin, V. Kachanov, V. Kutyin, J.-P. Peigneux, A. Petrukhin *et al.*, Absorption cross-sections of 25 GeV/c antideuterons in Li, C, Al, Cu and Pb, Phys. Lett. **31B**, 230 (1970).

[115] E. Abbas *et al.* (ALICE Collaboration), Mid-rapidity anti-baryon to baryon ratios in pp collisions at $\sqrt{s} = 0.9, 2.76$ and 7 TeV measured by ALICE, Eur. Phys. J. C **73**, 2496 (2013).

[116] K. Aamodt *et al.* (ALICE Collaboration), Midrapidity Antiproton-to-Proton Ratio in pp Collisions at $\sqrt{s} = 0.9$ and 7 TeV Measured by the ALICE Experiment, Phys. Rev. Lett. **105**, 072002 (2010).

[117] S. Acharya *et al.* (ALICE Collaboration), Production of (anti-)^{3}He and (anti-)^{3}H in p-Pb collisions at $\sqrt{s_{\rm NN}} =$ 5.02 TeV, Phys. Rev. C **101**, 044906 (2020).

[118] S. Acharya *et al.* (ALICE Collaboration), Production of ^{4}He and $^4\overline{\rm He}$ in Pb-Pb collisions at $\sqrt{s_{\rm NN}} = 2.76$ TeV at the LHC, Nucl. Phys. **A971**, 1 (2018).

[119] S. Acharya *et al.* (ALICE Collaboration), Multiplicity dependence of light (anti-)nuclei production in p-Pb collisions at $\sqrt{s_{\rm NN}} = 5.02$ TeV, Phys. Lett. B **800**, 135043 (2020).

[120] S. Acharya *et al.* (ALICE Collaboration), (Anti-)deuteron production in pp collisions at $\sqrt{s} = 13$ TeV, Eur. Phys. J. C **80**, 889 (2020).

[121] A. Auce, R. F. Carlson, A. J. Cox, A. Ingemarsson, R. Johansson, P. U. Renberg, O. Sundberg, and G. Tibell, Reaction cross-sections for 38, 65, and 97 MeV deuterons on targets from ^{9}Be to ^{208}Pb, Phys. Rev. C **53**, 2919 (1996).

[122] J. Jaros, A. Wagner, L. Anderson, O. Chamberlain, R. Z. Fuzesy, J. Gallup, W. Gorn, L. Schroeder, S. Shannon, G. Shapiro *et al.*, Nucleus-nucleus total cross-sections for light nuclei at 1.55 GeV/c/nucleon and 2.89 GeV/c/nucleon, Phys. Rev. C **18**, 2273 (1978).

[123] S. Agostinelli *et al.* (GEANT4 Collaboration), GEANT4–a simulation toolkit, Nucl. Instrum. Methods Phys. Res., Sect. A **506**, 250 (2003).

[124] V. Uzhinsky, J. Apostolakis, A. Galoyan, G. Folger, V. M. Grichine, V. N. Ivanchenko, and D. H. Wright, Antinucleus-nucleus cross sections implemented in GEANT4, Phys. Lett. B **705**, 235 (2011).

[125] P. A. Zyla *et al.* (Particle Data Group), Review of particle physics, Prog. Theor. Exp. Phys. **2020**, 083C01 (2020).

[126] L. C. Tan and L. K. Ng, Calculation of the equilibrium anti-proton spectrum, J. Phys. G **9**, 227 (1983).

[127] M. Stref and J. Lavalle, Modeling dark matter subhalos in a constrained galaxy: Global mass and boosted annihilation profiles, Phys. Rev. D **95**, 063003 (2017).